Energy Efficient COGnitive MAC for Sensor Networks under WLAN Co-existence – Revised complementary technical report

Ioannis Glaropoulos
12 April 2014

***Abstract*—Energy efficiency has been the driving force behind the design of communication protocols for battery-constrained wireless sensor networks (WSNs). The energy efficiency and the performance of the proposed protocol stacks, however, degrade dramatically in case the low-powered WSNs are subject to interference from high-power wireless systems such as WLANs. In this paper we propose COG-MAC, a novel cognitive medium access control scheme (MAC) for WSNs that minimizes the energy cost for multihop communications, by deriving energy-optimal packet lengths and single-hop transmission distances based on the experienced interference from the WLAN. We evaluate COG-MAC by deriving a detailed analytic model for its performance and by comparing it with previous access control schemes. Numerical and simulation results show that a significant decrease in energy cost, up to 66%, can be achieved in a wide range of scenarios, particularly under severe WLAN interference. COG-MAC is, also, lightweight and shows high robustness against WLAN model estimation and WSN schedule synchronization errors. COG-MAC is, therefore, an effective, implementable solution to reduce the WSN performance impairment when coexisting with WLANs.**

***Index Terms*—WSN, energy efficiency, cognitive networks, coexistence.**

I. Introduction

THE increasing number of different wireless technologies sharing the open spectrum bands, such as the 2.4GHz ISM band, demands for a rethinking of the protocols regulating the spectrum access. As the medium access control (MAC) schemes are carefully designed for one given technology, they are not anymore able to achieve the objective of efficient and "fair" sharing of the wireless resources when operating under interference from heterogeneous technologies.

In this paper we consider the specific case of the coexistence of IEEE 802.11 wireless local area networks (WLANs) and IEEE 802.15.4-compliant wireless sensor networks (WSNs). Both technologies apply carrier sensing-based medium access control with collision avoidance. In addition, WSNs try to locate the narrow frequency band with less harmful interference for their operations. Unfortunately, all these techniques do not avoid high interference and frequent packet losses in the WSN, which are mainly caused by the significantly different transmission bandwidths and powers of the two technologies competing for the same resource.

As shown in [1], the WLAN terminals operate in a relatively broad channel and at a higher transmission power than WSNs. Therefore, they are *blind* to the narrow-band, low-powered WSN transmissions, and do not back off when a transmission is initiated that overlaps with that of the WSN packet being transmitted. In all this, the WLAN transmissions remain basically unaffected by the low WSN interference, while WSN packets are lost. Fortunately, measurement results show that the WLAN traffic is rather bursty with long *white spaces*, when the channel is idle because all WLAN users are inactive [2]. Therefore, in order to maximize its performance, the WSN should be able to transmit in these long interference-free times, being cognitive of the radio environment as imposed by the WLAN activity.

In this paper we propose and evaluate a new duty-cycled COGnitive MAC (COG-MAC) protocol for wireless sensor networks, which extends the IEEE 802.15.4 MAC and aims at minimising the energy loss due to unsuccessful transmissions over the interfered channel. Our paper provides the following contributions. 1) We give a characterization of the WLAN channel usage patterns as seen by the sensor nodes, taking into account the nodes' limited channel estimation capabilities, and propose techniques for distributed WLAN usage pattern estimation. 2) Based on these results we design COG-MAC, that optimizes the packet length and the transmission distance, and performs WLAN activity-aware channel access to ensure that WSN nodes transmit in the long WLAN white space periods. 3) We provide an accurate analytical model that describes the probability of COG-MAC packet transmission success. We use the model to optimize the WSN packet size and the single-hop WSN transmission distance to minimize the *normalized transmission energy cost* metric, which we define as the energy required to successfully transmit a unit of information over a unit of distance. 4) We show that all the basic components of COG-MAC are essential for achieving the objective of energy efficient communication, and COG-MAC, compared to previous access schemes, can reduce the normalized energy cost up to 66%, and can significantly decrease the end-to-end energy cost in a multihop WSN without increased delay.

The rest of the paper is organized as follows. Related work is presented in Section II. Section III describes the networking scenario and the interference and sensing models and Section IV gives the WLAN channel activity model. In Section V we describe the proposed protocol stack, followed by its mathematical analysis in Section VI. In Section VIII we present a numerical evaluation of COG-MAC along with a comparison with traditional WSN MAC schemes, while a simulation study is presented in Section IX. We conclude the

paper in Section X.

II. Related Work

Energy efficient communications have been extensively studied for single WSNs operating in some geographical area [3][4]. The key concept for energy efficiency in sensor networks is duty-cycling, that is, letting the sensors turn off their radios whenever idle [5][6][7]. Energy efficiency can be further improved by the co-optimization of duty-cycle length, MAC, data link, routing and transport layer protocols [8][9][10].

It is recognized, however, that cross-network interference can have significant effect on the network performance, as it is shown for coexisting WSNs in [11] and for WLAN and Bluetooth interference in [12][13]. WSN multi-channel operation aims at avoiding this cross-network interference, or at minimizing its effect, by letting the network, or the individual nodes, tune to the best available band for communication [14][15][16]. These solutions are efficient as long as there exist channels with no or low interference, but lose effectiveness when all considered channels suffer from interference with similar statistical behavior.

Therefore, as wireless channels are getting densely populated, it is important to design protocols that can work efficiently even in the presence of cross-network interference. Many of the proposed solutions build on the known characteristics of the interfering networks. The transmission characteristics of WLANs is modified in [17] with narrowband sensing, with additional HW cost, and in [18], where the sensors force the WLAN to back off by sending frequent (one per DIFS), short, high power jamming signals during their packet transmission, which needs complex PHY layer and leads to increased energy consumption in the WSN, even at low WLAN load. Instead, the effect of interference is minimized without changing the WLAN behaviour in [19] and [20] introducing packet header and payload redundancy optimized for known partial collision patterns.

Recent works investigate how to avoid WLAN interference by employing channel availability predictions. The case of a non-saturated single WLAN AP is studied in [21], modeling the packet arrivals at the users as a Bernoulli process. In [22] a Poisson arrival process is considered, and WLAN output buffers are modeled as M/G/1 queues, resulting in sub-geometric idle period distribution. While these models capture the effect of the WLAN MAC, their generality is limited, since they are based on simple, rather unrealistic traffic models.

To capture the effect of realistic network load, [2][23][24] use traffic traces to find the distribution of WLAN idle periods. These results show that idle periods can be short contention periods, in the range of hundreds of microseconds, or heavy-tailed white spaces, where WLAN users are inactive. The average white space length depends on the WLAN load and is in the range of tens of milliseconds. In [25] similar results are derived based on the self-similar nature of WLAN traffic.

Considering the long transmission times in the WSN, it is important to capture the heavy-tail characteristics of the WLAN channel usage. Therefore, in our work we apply the model of [2][26] where a mixture distribution is proposed to model the idle periods, capturing the two basic sources of inactivity, the long heavy-tailed white space periods, when the WLAN users are inactive, and the short contention windows. Given this WLAN channel usage model we claim that the WSN on one hand needs to avoid channel access in the contention windows and on the other hand it needs to optimize transmissions in the long white space periods [27], which are the key functions in the proposed COG-MAC.

III. Networking Scenario, Interference and Sensing Models, Extended

We consider a WLAN Access Point (AP) zone under which a IEEE 802.15.4-compliant WSN is deployed. The WSN nodes are battery-powered and operate on a single 5MHz channel inside the 2.4GHz ISM band. They transmit information over multiple hops, and are able to estimate the distance to their neighboring nodes [28].

WLAN users are distributed inside the AP zone and operate on a 802.11 22MHz channel, covering the WSN channel. The WLAN transmission power is in the order of 15-20dBm. The WLAN terminals are blind to the WSN nodes [25], that is, the WLAN carrier-sense mechanism does not detect the low-power WSN signals, which results in collisions, and hence packet losses in the WSN. On the opposite side, the WSN nodes transmit with a signal power that is in the order of 0-3dBm [29] and, thus, their impact on WLAN operation is negligible [23]. Therefore, to ensure efficient WSN communication, sensor nodes need to consider the WLAN activity when transmitting. In the remainder of this section we clarify our assumptions on the interference and sensing models used throughout the paper.

The signal propagation is assumed to be adequately described by a simple path-loss model. In order to correctly receive a packet, a WSN node needs to receive it with Signal to Interference plus Noise Ratio (SINR) above a given threshold, denoted as ζ_{SINR}, where the interference is caused by a single active WLAN transmitter. Considering a WSN pair of nodes with r being the distance between the transmitting and receiving sensor. Based on the path-loss attenuation model, the resulting SINR, assuming a WLAN interferer at distance R_I from the receiving sensor will be

$$\boldsymbol{\zeta}_{\text{SINR}} = \frac{P_{\text{WSN}} P_{L_0} r^{-\eta}}{P_{\text{WLAN}} P_{L_0} R_I^{-\eta} + \sigma_N^2}$$

where η is the channel path-loss exponent, P_{WSN} is the WSN transmission power, P_{WLAN} is the fraction of WLAN transmission power inside the narrow WSN band, and P_{L_0} and σ_N^2 denote the attenuation at 1m reference distance and the noise (AWGN) power, respectively. The WLAN interference results in WSN packet reception error, if $\boldsymbol{\zeta}_{\text{SINR}} \geq \zeta_{\text{SINR}}$. This results in circular interference zones around receiving sensors, with radius R_I [30]:

$$R_I(r, \zeta_{\text{SINR}}, \eta, P_{\text{WSN}}, P_{\text{WLAN}}) = \sqrt[\eta]{\frac{\zeta_{\text{SINR}} P_{\text{WLAN}} P_{L_0}}{P_{\text{WSN}} P_{L_0} r^{-\eta} - \zeta_{\text{SINR}} \sigma_N^2}}, \quad (1)$$

Whenever an overlap occurs between a WSN packet transmission and a WLAN transmission within the receiving sensor node interference zone of radius R_I, we assume that the WSN packet is lost.

The WSN nodes perform channel sensing based on energy detection through their build-in Receiver Signal Strength Indicator (RSSI) [29]. In the proposed system two kinds of sensing are performed. Repeated sensing over long periods of time for WLAN activity model estimation, and short-time sensing for channel access control. The performance of both kinds of sensing is bounded by the *maximum sensitivity level* ψ_0 of the sensor, stating the minimum signal level that can be detected [29]. Short sensing time leads to probabilistic energy detection, characterised by the probability of *missed detection*, p_{MD}, when a signal is not detected, and the probability of *false alarm*, p_{FA}, when the sensing results in "signal detected" decision, even when the channel is idle [31]. The false alarm probability p_{FA} is a function of the sensing time t_s and of the energy decision threshold γ, and can be calculated as the probability that the received AWGN energy is above the decision threshold:

$$p_{\text{FA}}(t_s;\gamma) \triangleq \mathcal{Q}\left(\frac{\gamma-\sigma_N^2}{\sqrt{2\sigma_N^4/f_s t_s}}\right)$$

where $\mathcal{Q}$ denotes the complementary Gaussian CDF function, and f_s denotes the sampling frequency, thus $f_s \cdot t_s$ denotes the number of samples aggregated at the energy detector [32]. In this paper we consider a target p_{FA} which gives γ as [31]:

$$\gamma(p_{\text{FA}}) = \max\left\{\psi_0, \sigma_N^2\left[1+\sqrt{2/(f_s t_s)}\mathcal{Q}^{-1}(p_{\text{FA}})\right]\right\}. \quad (2)$$

The missed detection probability, p_{MD}, depends on the received signal power, $P_{Rx}(d)$, given as a function of the distance to the transmitter d, namely, $P_{Rx}(d) = P_{\text{WLAN}} P_{L_0} d^{-\eta}$. It also depends on the decision threshold, γ, which in turn is determined, using (2), by the target p_{FA}:

$$p_{\text{MD}}(t_s, d; \gamma(p_{\text{FA}})) = 1 - \mathcal{Q}\left(\frac{\gamma(p_{\text{FA}}) - (\sigma_N^2 + P_{Rx}(d))}{\sigma_N^2\sqrt{2/(f_s t_s)}}\right). \quad (3)$$

During the long-period sensing the sensors keep measuring the channel to collect samples of active and idle period durations. Due to the longer sensing time, p_{FA} approaches zero. The missed detection probability p_{MD} also approaches zero inside the sensors $\mathcal{A}_{\text{CCA}}$, the CCA area, where all transmissions are detected, and approaches 1 outside the $\mathcal{A}_{\text{CCA}}$.

Under the path-loss propagation model the CCA area is circular; its radius depends on the WLAN transmission power and can be controlled by tuning the CCA threshold $\psi \geq \psi_0$ [29]:

$$R_{\text{CCA}} \triangleq R_{\text{CCA}}(\psi) = \left[(\psi-\sigma_N^2)/(P_{\text{WLAN}} P_{L_0})\right]^{-1/\eta}. \quad (4)$$

We derive the COG-MAC performance model considering path-loss-based channel attenuation. However, the model can be extended for more generic signal attenuation models, at the expense of increased analytic complexity. In [33] we give the extended model, based on channel attenuation enhanced with log-normal shadowing, and evaluate the effect of shadowing on the protocol performance in Section VIII.

IV. The WLAN Channel Activity Model

The WLAN channel activity can be modeled as a semi-Markovian system of active and idle periods as originally proposed in [23]. We call this model the *Global View*, since it captures the global WLAN activity. Fig. 1(a) depicts the states of the Global View model and their merging into a two-state semi-Markovian chain. The states of Data, SIFS and ACK transmissions are grouped together into a single *Active* state and the states that represent the WLAN Contention Window period (CW) and the WLAN *white space* (WS) due to user inactivity are merged into a single *Idle* state. The distributions of the active and idle states, $f_A(t)$ and $f_I(t)$, respectively, define how long the WLAN channel remains in either state. As proposed in [23], a *uniform* distribution in a range $[\alpha_{\text{ON}}, \beta_{\text{ON}}]$ sufficiently models the active channel periods. The idle distribution is modeled as a *mixture* of uniformly distributed idle periods within $[0, \alpha_{\text{BK}}]$, corresponding to the WLAN contention periods, and long, zero-location *generalized Pareto*-distributed idle periods with parameters (ξ, σ) that capture the heavy-tailed behavior of the white spaces. The *percentage of contention periods* $p \in (0,1)$ determines the shape of the mixed idle distribution, which obtains the following form [23]:

$$f_I(t) \triangleq p f_I^{(\text{CW})}(t) + (1-p) f_I^{(\text{WS})}(t) = \\ = \begin{cases} p \cdot \frac{1}{\alpha_{\text{BK}}} + (1-p)\cdot\frac{1}{\sigma}(1+\xi\frac{t}{\sigma})^{-\frac{1+\xi}{\xi}}, & t \leq a_{\text{BK}}, \\ (1-p)\cdot\frac{1}{\sigma}(1+\xi\frac{t}{\sigma})^{-\frac{1+\xi}{\xi}}, & t > a_{\text{BK}}, \end{cases} \quad (5)$$

while the active distribution is given as:

$$f_A(t) = 1/(\beta_{\text{ON}} - \alpha_{\text{ON}}), \quad t \in (\alpha_{\text{ON}}, \beta_{\text{ON}}). \quad (6)$$

We define the WLAN *load* as the percentage of time the channel is active due to WLAN operation:

$$\rho \triangleq \frac{E[T_{\text{ON}}]}{E[T_{\text{ON}}] + E[T_{\text{OFF}}]} = \frac{\frac{\alpha_{\text{ON}}+\beta_{\text{ON}}}{2}}{p\frac{\alpha_{\text{BK}}}{2} + (1-p)\frac{\sigma}{1-\xi}}. \quad (7)$$

Additionally, this provides the probabilities of active and idle channel at an arbitrary point in time, $p_A = \rho$ and $p_I = (1-\rho)$, respectively.

Our objective is that of estimating the parameters of the model by means of sensor node observations. To this purpose, we define a *Local View* model by "extracting" from the Global View the WLAN channel activity as seen by a single sensor node. Due to sensitivity limitations the sensors detect WLAN transmitters only within the CCA area, that is, they observe the WLAN activity only partially, with some probability, given by the observable load parameter p_{CCA}. Assuming uncorrelated consequent WLAN transmissions the channel activity pattern seen by a sensor can be described with a 3-state semi-Markovian system, as shown in Fig. 1(b), distinguishing between detected and non-detected WLAN activity that occur with probabilities, p_{CCA} and $1-p_{\text{CCA}}$, respectively. Finally, by merging the states at which the sensor detects an idle channel we obtain the *Local View*, as a 2-state semi-Markovian system with the *observable* sojourn time distributions $f_{\tilde{A}}(t)$ and $f_{\tilde{I}}(t)$. It holds that $f_{\tilde{A}}(t) = f_A(t)$, but $f_{\tilde{I}}(t) \neq f_I(t), \quad \forall p_{\text{CCA}} < 1$. The observable idle channel period consists of a random number of WLAN *cycles*, that is,

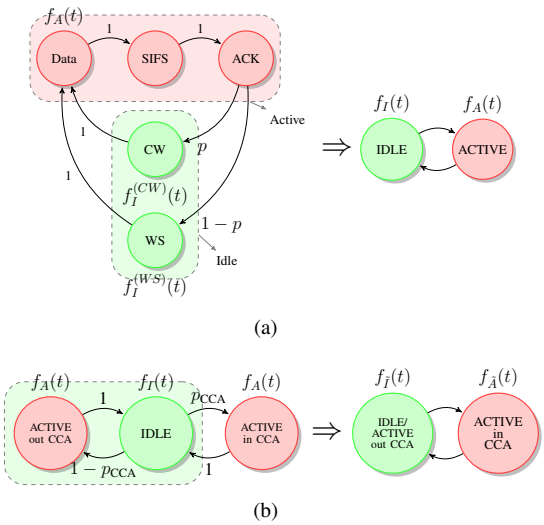

Fig. 1. (a): The Global View model with all channel states and the reduced two-state semi-Markovian model. (b): The 3-state semi-Markovian model and its 2-state equivalent for the Local View channel usage modeling.

consecutive idle and un-detected active periods, followed by an additional idle period. Its distribution, $f_{\bar{I}}(t)$, is, therefore, a random-term convolution-based function of the idle and active time distributions, $f_I(t)$ and $f_A(t)$, and of the observable load p_{CCA}, and can be expressed in closed form only in the Laplace transform (LT) domain, as shown in [34]:

$$f_{\bar{I}}^*(s) = f_I^*(s) \cdot p_{\text{CCA}} \;/\; \left[1-(1-p_{\text{CCA}})f_I^*(s)f_A^*(s)\right], \quad (8)$$

where $f^*(s)$ denotes the Laplace transform of function f. We discuss the feasibility of parameter estimation in [34][35], where we propose an estimation algorithm that integrates dynamically the collected samples, and therefore runs efficiently on memory-constrained sensor devices.

V. The Cognitive WSN

We propose a WSN COGnitive Medium Access Control (COG-MAC) that employs WLAN usage prediction and channel sensing so as to minimize the energy cost for *unicast* WSN communication under WLAN interference. In particular, it aims at minimizing the transmission energy spent by sensors for communicating.

The operation of COG-MAC is divided into two main phases. The first one is the *estimation and optimization phase*, when a sensor listens to the channel and gathers samples of the active and idle times, estimates the Local View parameters and selects the optimal one-hop transmission distance and the optimal packet size. The second one is the *transmission phase*, when the sensor transmits and receives information following a duty-cycled cognitive MAC protocol, adopting a variant of the IEEE 802.15.4 MAC. The sensor moves back to the first phase either periodically, or when it experiences a performance drop, suggesting that the estimated WLAN activity parameters are no longer valid (i.e., WLAN activity has significantly changed).

A. Estimation and optimization

During the estimation phase potential transmitter (TR) and receiver (RR) sensors listen to the channel and gather active

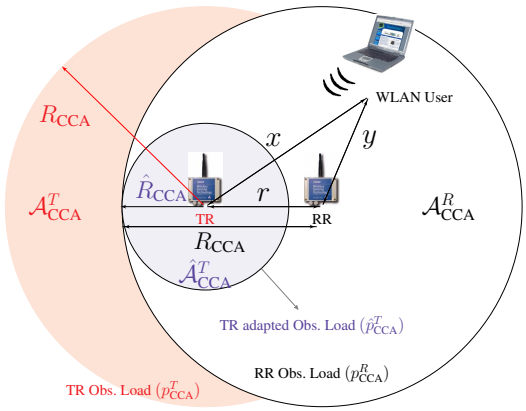

Fig. 2. TR and RR CCA areas, $\mathcal{A}^T_{\text{CCA}}$ and $\mathcal{A}^R_{\text{CCA}}$, and the adapted CCA area $\hat{\mathcal{A}}^T_{\text{CCA}}$.

and idle times for estimating the WLAN channel activity. As shown in Fig. 2, they perform the measurements for the maximized CCA area $\mathcal{A}_{\text{CCA}}$ (denoted by $\mathcal{A}^T_{\text{CCA}}$ and $\mathcal{A}^R_{\text{CCA}}$ for TR and RR respectively) by using the maximum sensitivity level ψ_0, leading to $R_{\text{CCA}} = R_{\text{CCA}}(\psi_0)$. Based on these measurements they derive the Local View parameters, that is, the parameters of the functions $f_A(t), f_I(t)$, and p_{CCA}. The required number of the samples and thus the length of the estimation phase depends on the target estimation accuracy, which in turn is determined by the sensitivity of COG-MAC. Therefore, we discuss this issue in Section VIII.

In addition, for a better estimate of the spatial distribution of the active WLAN users, each sensor also evaluates $\hat{p}^T_{\text{CCA}}$, the common load it can observe within the overlap of the CCA areas. Specifically, it measures the load in the disk area $\hat{\mathcal{A}}^T_{\text{CCA}}$ by filtering the measurements with a changed sensitivity level ψ, such that for a TR–RR distance r, $\hat{R}_{\text{CCA}} = R_{\text{CCA}} - r$. At the end of the estimation phase the sensors receive the observable load values from the potential receivers, denoted by p^R_{CCA}. Based on the locally estimated and received WLAN channel activity model parameters, the sensors select the transmission parameters that are expected to result in minimum energy consumption per bit and meter, according to the model and the implementation given in Section VI. Specifically, they optimize the packet size, to trade-off the probability of interference with a new WLAN transmission and the useful information transmitted per packet. They optimize the transmission distance, to trade-off the probability that a new WLAN transmission does not cause harmful interference and WSN packet transmission can continue even after the white space period, and the progression towards the multihop destination.

B. Transmissions with COG-MAC

The estimation and optimization phase is followed by the *transmission phase* when actual network operation occurs. We assume that the WSN operates under duty-cycling to limit the energy that is spent in idle listening [36][6]. WSN nodes synchronize their duty-cycles by employing a schedule synchronization protocol, the actual implementation of which is out of the scope of the paper. Synchronization gaps are,

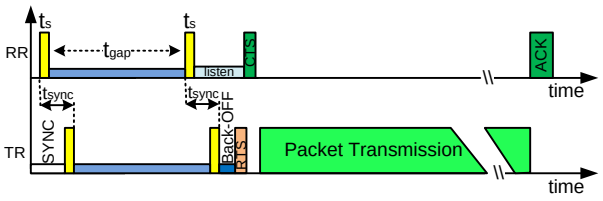

Fig. 3. Time diagram of COG-MAC operations.

however, expected, as a result of CPU clock drift, and have to be accounted for. Their maximum value $t_{\text{SYNC}}^{\max}$ is determined by the frequency of synchronization data exchange.

Fig. 3 shows the COG-MAC operation within a duty-cycle for potential transmitters (TR) and receivers (RR). The duty cycle of the TR nodes starts with a guard time (denoted as SYNC in the figure) equal to $t_{\text{SYNC}}^{\max}$, ensuring that channel sensing and transmission do not collide due to the lack of perfect synchronization. The medium access control is a modified CSMA/CA with the key component of dual channel sensing. As it is shown in Fig. 3, the *on* time of the duty cycle begins with two short channel sensing measurements with a duration of t_s, separated by a time *gap* of t_{gap}, where $\alpha_{\text{ON}} \geq t_{\text{gap}} \geq \alpha_{\text{BK}}$. If the channel state is correctly detected as idle at both measurements, the sensors can safely assume that the spectrum was idle in the entire time and characterize the idle period as a white space. The operation in the rest of the cycle is determined by the sensing result. If any of the measurements have indicated an active state, the sensor immediately transits to *sleep* mode to save energy. Sensors with idle measurements stay instead awake and follow a CSMA/CA channel access with RTS/CTS exchange. RTS/CTS has been shown to be beneficial in [27], as it allows TR and RR to share their view on the channel status, and increases the probability that the current period is indeed a long white-space (and not the case when a WLAN station is transmitting outside the CCA area), as the total observable load includes the percentage seen by the RR node. We evaluate the usefulness of RTS/CTS under fixed packet size in Section VIII. Sensors transit to sleep mode after packet transmission, according to the employed duty-cycle protocol.

VI. COG-MAC Optimization

In this section we define the COG-MAC energy consumption model and formulate the packet size and transmission distance optimization problem.Then we present the detailed analytic model of COG-MAC that is required for the optimization. In order to focus on the effect of WLAN interference, we consider the case of low WSN load, when the probability of sensors competing for the channel is low. The model can be extended for the high load case, including expected delays of channel access due to contention resolution.

A. Energy efficiency optimization

COG-MAC consumes energy for computing and storing the optimal transmission parameters, for packet transmission and for listening and packet reception. Below we focus on the energy spent for transmission, as the energy consumption of computation in typical sensor nodes is at least two orders of magnitude less than that of communication. For simplicity we do not consider the energy spent at the receiver (for listening and reception); the energy model can, however, be directly extended to include these costs. We consider the WSN communication energy optimal when the energy cost of transmitting a unit of information at unit distance is minimized. Therefore we define the main performance measure as the energy consumption at the TR until successful packet delivery, that is, through the sequence of possibly unsuccessful and eventually successful RTS/CTS *handshake* and packet transmission attempts, normalized by the amount of information transmitted and the distance covered.

We consider a fixed power cost, $P_{\text{ON}}^{\text{WSN}}$, for channel sensing, transmitting and listening for CTS reception. Consequently, the TR energy cost of attempting a handshake is $e_{\text{hs}} = P_{\text{ON}}^{\text{WSN}} t_{\text{hs}}$, where t_{hs} is the duration of the handshake. Let $\mathcal{T}$ denote the event of successful handshake. Assuming that the WLAN channel state is uncorrelated at the consecutive handshake attempts, the number of unsuccessful handshakes has geometric distribution with parameter $P\{\mathcal{T}$, and the expected energy cost until handshake success becomes:

$$E_{\text{hs}}(r) = e_{\text{hs}}/P\{\mathcal{T}\}. \tag{9}$$

The energy cost of packet transmission with transmission time t is, similarly, $P_{\text{ON}}^{\text{WSN}} t$. If a packet transmission attempt fails, a new handshake must be established before attempting a new transmission. Consequently, the expected energy cost of successful packet delivery with packet transmission time t becomes:

$$E_{\text{trans}}(r,t) = \left[E_{\text{hs}}(r) + P_{\text{ON}}^{\text{WSN}} \cdot t\right]/P\{\text{transmission success}|\mathcal{T}\}. \tag{10}$$

The theoretical optimal packet length and receiver distance, t^*, r^*, as a function of the parameters, $(\xi, \sigma, p, p_{\text{CCA}}, \hat{p}_{\text{CCA}}^T)$ is given by:

$$(t^*, r^*) = \arg\min_{t,r} \left\{E_{\text{trans}}(r,t)\left[r \cdot (R_{\text{WSN}} t - L_0)\right]\right\}, \tag{11}$$

where R_{WSN} and L_0 denote the WSN transmission rate and the packet overhead, respectively. (11) can be easily modified to consider only t or r WSNs with known node distance or packet size respectively.

We derive the optimal values numerically by solving the above optimization problems applying the bisection method. For practical implementation the optimization problem can be solved a-priori, and the optimal packet size and next-hop distance pairs for a set of WLAN load parameter vectors can be stored in the sensor.

B. COG-MAC probability of successful handshake and transmission

In this Section we derive analytically the probabilities of successful handshake and packet transmission, required in (9), (10), respectively.

The TR starts a handshake by transmitting an RTS packet, if its dual sensing process gave idle channel status. Let $\hat{I}_T^{(i)}, \hat{I}_R^{(i)}$ denote the events that the i-th channel measurement is idle

at the TR and RR nodes, respectively, with $i = 1, 2$. The handshake attempt is successful if the RR node is awake, as a result of a pair of idle measurements, and, additionally, if the communication is not disturbed by an ongoing, miss-detected WLAN transmission, or by a WLAN transmission that starts during the period of the handshake within the TR or RR interference regions. After a successful handshake the packet transmission itself will be successful, if all WLAN sources within the interference region of the RR remain silent during the whole packet transmission time.

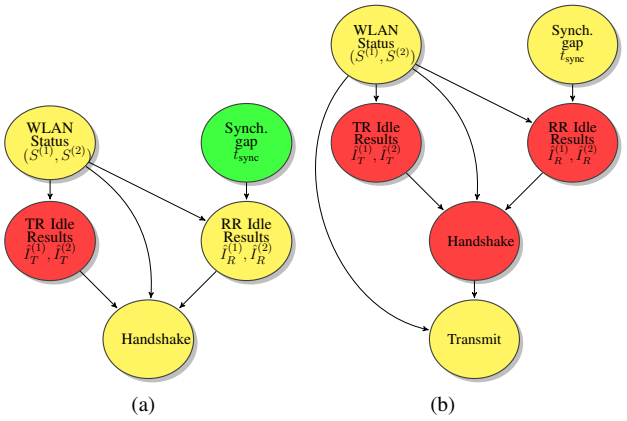

Fig. 4. Bayesian networks representing the causal relations in the handshake, (a), and transmission process, (b). With red color are the observed (instantiated) variables, that affect the variables in yellow, but not the ones in green.

The derivation of the probability of successful transmission is divided into five steps.

1) We define the spatial distribution of WLAN sources, as seen by the TR node, based on the a priori measured observable load values and the TR-RR distance r.
2) Using Bayesian inference we derive the probability of idle and active channel *status* at the TR and at the RR nodes, given the observed idle state measurements at the TR (Fig. 4(a)).
3) We derive the distribution of the interference-free time that remains after the dual sensing process.
4) Based on the previous steps, we express the probability of a successful handshake between the TR and the RR node (Figure 4(a)).
5) Finally, given the successful handshake, we express, using Bayesian inference, the probability of successful packet transmission as a function of transmission distance and packet length (Fig. 4(b)).

Let $S \in \mathcal{S} = \{I\} \cup \{A_{\text{XY}}(x, y) : x \in \mathcal{X}, y \in \mathcal{Y}\}$ be the channel status. The status is either idle, I, or active, $A_{\text{XY}}(x, y)$, with a WLAN *source* at distances $(X, Y) = (x, y) \in \mathcal{X} \times \mathcal{Y}$ from the TR and RR nodes, respectively (see Fig. 2). $\mathcal{X} \times \mathcal{Y}$ denotes the set of all possible WLAN source positions. $S^{(i)} \in \mathcal{S}$ denotes the channel status during the i-th sensing measurement, where $i = 1, 2$. $\hat{I}_T^{(i)}, \hat{I}_R^{(i)}$ denote the events that the i-th channel measurement is idle at the TR and RR nodes, respectively.

1) Spatial distribution of WLAN interfering sources: The spatial distribution of WLAN sources around the TR and RR nodes affects their miss-detection probabilities, as well as the probability that such a source within the TR/RR interference region starts to transmit during the WSN packet transmission.

As shown in Fig. 2, the TR can estimate the joint distribution of the distances X,Y of a possible active WLAN source based on the a-priori known observable load values, p_{CCA}^R, received from RR, and $\hat{p}_{\text{CCA}}^T$, measured by the TR itself. Since $\hat{\mathcal{A}}_{\text{CCA}}^T \subseteq \mathcal{A}_{\text{CCA}}^R$, an arbitrary WLAN source lies in the area $\hat{\mathcal{A}}_{\text{CCA}}^T$ with probability $\hat{p}_{\text{CCA}}^T$, in the area $\mathcal{A}_{\text{CCA}}^R \setminus \hat{\mathcal{A}}_{\text{CCA}}^T$ with probability $p_{\text{CCA}}^R - \hat{p}_{\text{CCA}}^T$, and in the AP area outside $\mathcal{A}_{\text{CCA}}^R$ otherwise. Since there is no additional a-priori information available about the WLAN source locations, the TR assumes that these sources are located uniformly at random inside the respective areas. In addition, we approximate the AP area as a disc around TR with radius $R_{\max}$. This approximation does not affect the model accuracy significantly, unless the TR happens to be very close to the border of the AP area.

Let $f_X(x)$ denote the unconditional probability density function of distance X, for uniformly random WLAN source locations in an area around TR, assuming a radius $R_{\max}$. Similarly, $f_{Y|X}(x, y)$ denotes the density of the distance Y from the RR node, given $X{=}x$, and $f_{XY}(x, y) = f_X(x) f_{Y|X}(x, y)$ denotes the unconditional joint distance density. These functions depend on the distance r between the two sensors and can be derived through basic geometry.

We aim at determining the distribution of distances X and Y, conditioned on the reported observable load values. First, conditioning on $\hat{p}_{\text{CCA}}^T$, we get:

$$p_{A_X}(x) = f_X(x) \cdot \begin{cases} \frac{\hat{p}_{\text{CCA}}^T}{\nu_{\hat{R}_{\text{CCA}}}}, & x \le \hat{R}_{\text{CCA}}, \\ \frac{1-\hat{p}_{\text{CCA}}^T}{1-\nu_{\hat{R}_{\text{CCA}}}}, & \text{otherwise} \end{cases}$$

where $\nu_{\hat{R}_{\text{CCA}}}, \nu_{R_{\text{CCA}}}$ denote the ratio of the observable areas $\hat{\mathcal{A}}_{\text{CCA}}^T$ and $\mathcal{A}_{\text{CCA}}^R$, respectively, over the total WLAN AP area with radius $R_{\max}$. Conditioned, additionally, on p_{CCA}^R, we get the following expression for the density function of X:

$$\begin{aligned} p_{A_X}(x) &= \\ &= f_X(x) \cdot \begin{cases} \frac{\hat{p}_{\text{CCA}}^T}{\nu_{\hat{R}_{\text{CCA}}}}, & x \le \hat{R}_{\text{CCA}}, \\ \frac{F_{Y|X}(x, R_{\text{CCA}})(p_{\text{CCA}}^R - \hat{p}_{\text{CCA}}^T)}{\nu_{R_{\text{CCA}}} - \nu_{\hat{R}_{\text{CCA}}}} + & \\ \quad + \frac{\overline{F}_{Y|X}(x, R_{\text{CCA}})(1-p_{\text{CCA}}^R)}{1-\nu_{R_{\text{CCA}}}}, & \text{otherwise.} \end{cases} \end{aligned} \tag{12}$$

Similarly, the conditional distance density $p_{A_{Y|X}}(x, y)$, can be expressed as:

$$\begin{aligned} p_{A_{Y|X}}(x, y) &= \\ f_{Y|X}(x, y) \cdot &\begin{cases} \frac{\hat{p}_{\text{CCA}}^T}{\nu_{\hat{R}_{\text{CCA}}}}, & x \le \hat{R}_{\text{CCA}} \\ \frac{p_{\text{CCA}}^R - \hat{p}_{\text{CCA}}^T}{\nu_{R_{\text{CCA}}} - \nu_{\hat{R}_{\text{CCA}}}}, & x > \hat{R}_{\text{CCA}}, y \le R_{\text{CCA}} \\ \frac{1-p_{\text{CCA}}^R}{1-\nu_{R_{\text{CCA}}}}, & \text{otherwise,} \end{cases} \end{aligned} \tag{13}$$

and the joint probability function, $p_{A_{\text{XY}}}$, as:

$$p_{A_{\text{XY}}}(x, y) = f_X(x) \cdot p_{A_{Y|X}}(x, y). \tag{14}$$

The density function of the distance Y is finally determined as the marginal density of the joint function $p_{A_{\text{XY}}}$:

$$p_{A_Y}(y) = \int_{\mathcal{X}} p_{A_{\text{XY}}}(x, y) dx. \tag{15}$$

2) Bayesian inference of channel status: We derive now the *posterior* distribution of channel status, $\left(S^{(1)}, S^{(2)}\right)$, given the observed TR idle measurements, applying Bayesian formulation. Conditioned on the idle channel measurements at the TR, the channel status distribution is determined by the false alarm and missed detection probabilities, which in turn depend on the distance between the TR and the active WLAN source.

To calculate $P\{\left(S^{(1)}, S^{(2)}\right)|\hat{I}_T^{(1)}, \hat{I}_T^{(2)}\}$ we use the following decomposition:

$$\begin{aligned} &P\{\left(S^{(1)}, S^{(2)}\right)|\hat{I}_T^{(1)}, \hat{I}_T^{(2)}\} = \\ &= P\{S^{(1)}|\hat{I}_T^{(1)}, \hat{I}_T^{(2)}\} \cdot P\{S^{(2)}|S^{(1)}, \hat{I}_T^{(1)}, \hat{I}_T^{(2)}\} = \\ &= P\{S^{(1)}|\hat{I}_T^{(1)}\} \cdot P\{S^{(2)}|S^{(1)}, \hat{I}_T^{(2)}\}. \end{aligned} \tag{16}$$

Conditioned on the first idle measurement the channel status is either idle or active with the following probabilities:

$$P\{I^{(1)}|\hat{I}_T^{(1)}\} = \frac{(1-p_{\text{FA}})p_I}{\int_{\mathcal{X}} p_{\text{MD}}(u)p_{A_X^{(1)}}(u)du + (1-p_{\text{FA}})p_I}, \tag{17}$$

$$P\{A_X^{(1)}|\hat{I}_T^{(1)}\} = \frac{p_{\text{MD}}(x)p_{A_X^{(1)}}(x)}{\int_{\mathcal{X}} p_{\text{MD}}(u)p_{A_X^{(1)}}(u)du + (1-p_{\text{FA}})p_I} \tag{18}$$

$$P\{A_{\text{XY}}^{(1)}|\hat{I}_T^{(1)}\} = \frac{p_{\text{MD}}(x)p_{A_{\text{XY}}^{(1)}}(x,y)}{\iint_{\mathcal{XY}} p_{\text{MD}}(u)p_{A_{\text{XY}}^{(1)}}(u,v)dudv + (1-p_{\text{FA}})p_I} \tag{19}$$

where $p_{A_X^{(1)}}(x) = p_A \cdot p_{A_X}(x)$ is the probability that a WLAN source is active at a distance x from the TR at the time of the first measurement, and $p_{A_{\text{XY}}^{(1)}}(x,y) = p_A \cdot p_{A_{\text{XY}}}(x,y)$ is the probability that it is active at distances x, y from TR and RR respectively.

To derive the second term of (16), we first express the status transition probabilities, $P\{S^{(2)}|S^{(1)}\}$, following Fig. 5.

For $I^{(1)}$ (Fig. 5(a),(c)):

$$P\{I^{(2)}|I^{(1)}\} = \overline{F}_{R_I}(t_{\text{gap}}), \tag{20}$$

$$P\{A_{\text{XY}}^{(2)}|I^{(1)}\} = \left(1 - P\{I^{(2)}|I^{(1)}\}\right) p_{A_{\text{XY}}}(x,y). \tag{21}$$

In the above, $F_{R_I}(t)$ denotes the distribution function of the remaining idle time, T_{R_I}, As the time of the first measurement is uniformly distributed within the WLAN idle period: $F_{R_I}(t) = \int_t^\infty (1-\frac{t}{z}) f_I(z)dz$. Similarly, for $S^{(1)} = A_{\text{XY}}^{(1)}$, $\forall x, y$ we obtain (Fig. 5(b)):

$$P\{I^{(2)}|A_{\text{XY}}^{(1)}\} = \int_0^{t_{\text{gap}}} \overline{F}_I(t_{\text{gap}} - z) f_{R_A}(z)dz, \tag{22}$$

with $f_{R_A}(t) = \int_t^\infty \frac{1}{z} f_A(z)dz$ denoting the density of the remaining active WLAN period. For $S^{(2)} = A_{\text{XY}}^{(2)}(x,y)$ we need to distinguish between the cases of a continuous active period – with the same WLAN source being active – or that of a short idle period between the measurements (Fig. 5(d)):

$$\begin{aligned} P\{A_{\text{XY}}^{(2)}|A_{\text{XY}}^{(1)}(x_1,y_1)\} &= \overline{F}_{R_A}(t_{\text{gap}})\delta(x_1,y_1) + \\ &+ [1 - \overline{F}_{R_A}(t_{\text{gap}}) - P\{I^{(2)}|A_{\text{XY}}^{(1)}\}]p_{A_{\text{XY}}}(x,y) \end{aligned} \tag{23}$$

Finally, we define the channel status probabilities conditioned on the second idle measurement and based on the a-priori status transition probabilities calculated in (20)-(23):

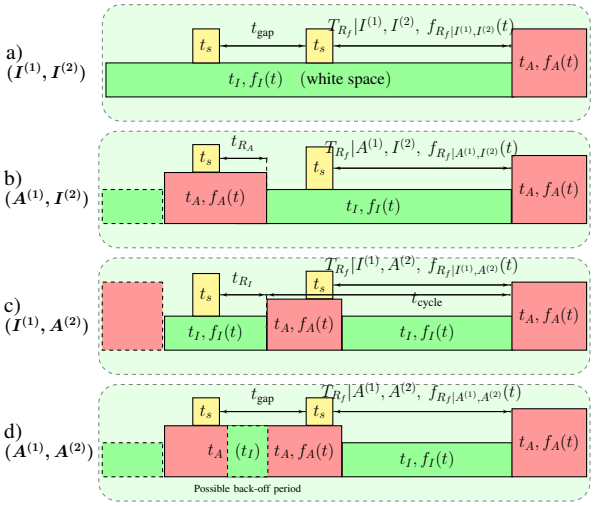

Fig. 5. Diagram for the calculation of remaining time densities.

$$\begin{aligned} &P\{I^{(2)}|I^{(1)}, \hat{I}_T^{(2)}\} = \\ &= \frac{(1-p_{\text{FA}})P\{I^{(2)}|I^{(1)}\}}{(1-p_{\text{FA}})P\{I^{(2)}|I^{(1)}\} + \int\int_{\mathcal{XY}} p_{\text{MD}}(u)P\{A_{\text{XY}}^{(2)}|I^{(1)}\}dudv}, \end{aligned} \tag{24}$$

$$P\{A_{XY}^{(2)}|I^{(1)}, \hat{I}_T^{(2)}\} = \left(1 - P\{I^{(2)}|I^{(1)}, \hat{I}_T^{(2)}\}\right) p_{A_{\text{XY}}}(x,y), \tag{25}$$

$$\begin{aligned} &P\{I^{(2)}|A_{XY}^{(1)}, \hat{I}_T^{(2)}\} = \\ &= \frac{(1-p_{\text{FA}})P\{I^{(2)}|A_{XY}^{(1)}\}}{(1-p_{\text{FA}})P\{I^{(2)}|A_{XY}^{(1)}\} + \int\int_{\mathcal{XY}} p_{\text{MD}}(u)P\{A_{XY}^{(2)}|A_{XY}^{(1)}\}dudv}, \end{aligned} \tag{26}$$

$$\begin{aligned} &P\{A_{XY}^{(2)}|A_{XY}^{(1)}(x_1,y_1), \hat{I}_T^{(2)}\} = \\ &= \frac{p_{\text{MD}}(x)P\{A_{XY}^{(2)}|A_{XY}^{(1)}(x_1,y_1)\}}{(1-p_{\text{FA}})P\{I^{(2)}|A_{XY}^{(1)}\} + \int\int_{\mathcal{XY}} p_{\text{MD}}(u)P\{A_{XY}^{(2)}|A_{XY}^{(1)}\}dudv}. \end{aligned} \tag{27}$$

3) Conditional remaining interference-free time: We define T_{R_F}, $T_{R_F}^{(\text{TR,RR})}$ as the total *interference-free time* remaining at the RR sensor and at both the TR and RR sensors, respectively, after the sensing process at the nodes, and derive the densities $f_{R_F|S^{(1)},S^{(2)}}(t)$, $f_{R_F|S^{(1)},S^{(2)}}^{(\text{TR,RR})}(t)$, given the channel status at the time of the TR measurements.

T_{R_F} includes the interval between the end of the second sensing measurement and the start of the following active WLAN period, and a *geometric* number of successive WLAN cycles, i.e. pairs of successive active and idle WLAN periods with density $f_C(t) = f_I(t) * f_A(t)$, representing WLAN transmissions outside the interference area.

Consequently, the distribution of T_{R_F} can be numerically calculated with the help of Laplace transformation, similar to (8) and for all $S^{(1)}, S^{(2)} \in \mathcal{S}$:

$$f_{R_F|S^{(1)},S^{(2)}}(t) = \mathcal{L}^{-1}\left\{\frac{p_{\mathcal{IN}} f_{R_f|S^{(1)},S^{(2)}}^*(s)}{1-(1-p_{\mathcal{IN}})f_I^*(s)f_A^*(s)}\right\}, \tag{28}$$

For additionally undisturbed TR, we obtain the density:

$$f_{R_F|S^{(1)},S^{(2)}}^{(\text{TR,RR})}(t) = \mathcal{L}^{-1}\left\{\frac{p_{\mathcal{IN}}^{(\text{TR,RR})} f_{R_f|S^{(1)},S^{(2)}}^*(s)}{1-(1-p_{\mathcal{IN}}^{(\text{TR,RR})})f_I^*(s)f_A^*(s)}\right\}, \tag{29}$$

where $p_{\mathcal{IN}}$, the probability that an activated WLAN source interferes with the RR reception is:

$$p_{\mathcal{IN}} = \begin{cases} p^R_{\text{CCA}}(\frac{R_{\mathcal{I}}(r)}{R_{\text{CCA}}})^2, & R_{\mathcal{I}}(r) \le R_{\text{CCA}} \\ p^R_{\text{CCA}} + (1-p^R_{\text{CCA}})\frac{R^2_{\mathcal{I}}(r)-R^2_{\text{CCA}}}{R^2_{\max}-R^2_{\text{CCA}}}, & \text{otherwise,} \end{cases} \quad (30)$$

and the probability that the source lies, additionally, inside the TR interference area is given as:

$$p^{(\text{TR,RR})}_{\mathcal{IN}} = \int_{y\le R_{\mathcal{I}}(r)}\int_{x\le R_{\mathcal{I}}(r)} p_{A_{\text{XY}}}(x,y)dxdy. \quad (31)$$

The interval between the end of the second sensing measurement and the start of the first active WLAN period is denoted by T_{R_f}, and its density depends on the channel status. In the derivations we approximate the sensing period as $T_s = 2t_s + t_{\text{gap}} \approx t_{\text{gap}}$, since $t_{\text{gap}} \gg t_s$.

For $\left(I^{(1)}, I^{(2)}\right)$ (Fig. 5(a)) we safely classify the idle period as white space, and consequently:

$$f_{R_f|I^{(1)},I^{(2)}}(t) = f_{R_I}(t+t_{\text{gap}})/\overline{F}_{R_I}(t_{\text{gap}}). \quad (32)$$

In the case $(A^{(1)}_{\text{XY}}, I^{(2)})$ (Fig. 5(b)), a transition from active to idle status occurs sometime $z \le t_{\text{gap}}$ after the first TR measurement, and the idle period may also be a back-off, which gives:

$$f_{R_f|A^{(1)}_{\text{XY}},I^{(2)}}(t) = \frac{1}{F_{R_A}(t_{\text{gap}})}\int_0^{t_{\text{gap}}} f_{R_A}(z)\frac{f_I(t+t_{\text{gap}}-z)}{\overline{F}_I(t_{\text{gap}}-z)}dz. \quad (33)$$

For $S^{(2)} = A^{(2)}_{\text{XY}}$ (Fig. 5(c)) the channel is active at the second measurement, and the remaining time, T_{R_f}, is given by the remaining active and the following idle period:

$$f_{R_f|I^{(1)},A^{(2)}_{\text{XY}}}(t) = \frac{1}{F_{R_I}(t_{\text{gap}})}\int_0^{t_{\text{gap}}} f_{R_I}(z)\frac{f_C(t+t_{\text{gap}}-z)}{\overline{F}_A(t_{\text{gap}}-z)}dz. \quad (34)$$

Finally under $(A^{(1)}_{XY}, A^{(2)}_{XY})$ (Fig. 5(d)), the active period may be continuous between the two measurements, or interrupted by a short idle time. In the case of continuous active period:

$$\begin{aligned} &f_{R_f|A^{(1)}_{XY}(x_1,y_1),A^{(2)}_{XY}(x_1,y_1)}(t) = \\ &= \frac{1}{\overline{F}_{R_A}(t_{\text{gap}})}\int_{t_{\text{gap}}}^{\infty} f_{R_A}(z)f_I(t+t_{\text{gap}}-z)dz, \end{aligned} \quad (35)$$

while in the case of a short idle period between the measurements, $(x_1,y_1) \ne (x_2,y_2)$:

$$\begin{aligned} &f_{R_f|A^{(1)}_{XY},A^{(2)}_{XY}}(t) = \frac{1}{\overline{F}_{R_A}(t_{\text{gap}})}\cdot \\ &\cdot\int_0^{t_{\text{gap}}} f_{R_A}(z_1)\frac{\int_0^{t_{\text{gap}}-z_1} f_I(z_2)}{F_I(t_{\text{gap}}-z_1)}\cdot\frac{f_{\text{cycle}}(t+t_{\text{gap}}-z_1-z_2)}{\overline{F}_A(t_{\text{gap}}-z_1-z_2)}dz_1dz_2. \end{aligned} \quad (36)$$

4) TR-RR handshake success: For a TR node aiming at communicating with an RR at distance r we calculate the probability of successful handshake, conditioned on the idle TR measurements. Let $\mathcal{T}$ denote the event of handshake success. $\mathcal{T}$ requires, first, idle measurements at the receiver, $\hat{I}^{(1)}_R, \hat{I}^{(2)}_R$. Second, it requires that no WLAN transmission interferes with the RTS/CTS handshake. Since the duration of the handshake is expected to be significantly lower than the WLAN activity dynamics, we approximate the second constraint as the requirement that all the possible active WLAN sources lie outside the interference regions of both the TR and the RR for the entire handshake period, t_{hs}:

$$P\{\mathcal{T}|S^{(1)},S^{(2)}\} = P\{\hat{I}^{(1)}_R,\hat{I}^{(2)}_R|S^{(1)},S^{(2)}\}\overline{F}^{(\text{TR,RR})}_{R_F|S^{(1)},S^{(2)}}(t_{\text{hs}}). \quad (37)$$

We begin with the case when the TR and RR duty cycles are perfectly synchronized. If the channel status is indeed idle during both of the TR measurements, i.e., $(S^{(1)},S^{(2)}) = (I^{(1)},I^{(2)})$, the handshake is successful if there is no false alarm at the RR, and the remaining interference-free time at both the RR and TR is longer than the total duration of the handshake, t_{hs}. That is:

$$P\{\mathcal{T}|I^{(1)},I^{(2)}\} = (1-p_{\text{FA}})^2\overline{F}^{(\text{TR,RR})}_{R_F|I^{(1)},I^{(2)}}(t_{\text{hs}}). \quad (38)$$

With a similar reasoning, the conditional handshake success probability for the remaining channel status cases becomes:

$$\begin{aligned} &P\{\mathcal{T}|A^{(1)}_{\text{XY}}(x,y),I^{(2)}\} = \\ &= (1-p_{\text{FA}})p_{\text{MD}}(y)\overline{F}^{(\text{TR,RR})}_{R_F|A^{(1)}_{\text{XY}},I^{(2)}}(t_{\text{hs}}),\ x\in\mathcal{X}, y\in\mathcal{Y} \end{aligned} \quad (39)$$

$$\begin{aligned} &P\{\mathcal{T}|I^{(1)},A^{(2)}_{XY}(x,y)\} = \\ &= (1-p_{FA})p_{\text{MD}}(y)\overline{F}^{(\text{TR,RR})}_{R_F|I^{(1)},A^{(2)}_{\text{XY}}}(t_{\text{hs}}),\ x,y\ge R_I(r), \end{aligned} \quad (40)$$

$$\begin{aligned} &P\{\mathcal{T}|A^{(1)}_{\text{XY}}(x_1,y_1),A^{(2)}_{\text{XY}}(x_2,y_2)\} = \\ &= p_{\text{MD}}(y_1)p_{\text{MD}}(y_2)\overline{F}^{(\text{TR,RR})}_{R_F|A^{(1)}_{\text{XY}},A^{(2)}_{\text{XY}}}(t_{\text{hs}}), x_2,y_2\ge R_I(r). \end{aligned} \quad (41)$$

The probability of handshake success is then calculated by averaging over all possible cases. (Eq. (42) on the top of next page.)

Let us, now, account for the possible synchronization offset between the schedules of the communicating sensors, described by the stochastic density f_{sync}.

In case the channel is idle during both TR measurements, $(S^{(1)},S^{(2)}) = (I^{(1)},I^{(2)})$, the sensing occurred in a white space period. Since the average duration of a white space is at least two orders of magnitude higher than the SYNC period in the WSN, it is unlikely that the RR conducts its first channel measurement outside the discovered white space period. Therefore, the handshake success probability can be approximately calculated as in (38).

For the other cases, however, due to the synchronization gap the TR and the RR may sense at different channel status. Let us consider that the channel status at the TR is $(S^{(1)},S^{(2)}) = (A^{(1)}_{XY}, I^{(2)})$.

First we compute the probability of the event $\left(\hat{I}^{(1)}_R,\hat{I}^{(2)}_R\right)|A^{(1)}_{\text{XY}},I^{(2)},z$ of idle RR measurements when the channel status transition occurs at time $t_{R_A} = z$ after the first TR measurement (Fig. 5(b)). We have

$$\begin{aligned} g(z) &\triangleq P\{\hat{I}^{(1)}_R,\hat{I}^{(2)}_R|A^{(1)}_{\text{XY}},I^{(2)},z\} = \\ &= \int_0^{t^{\max}_{\text{sync}}} P\{\hat{I}^{(1)}_R,\hat{I}^{(2)}_R|A^{(1)}_{\text{XY}},I^{(2)},z,t\}f_{\text{sync}}(t)dt, \end{aligned} \quad (43)$$

where $P\{\hat{I}^{(1)}_R,\hat{I}^{(2)}_R|A^{(1)}_{\text{XY}},I^{(2)},z,t\}$ denotes the probability of RR idle measurements when the synchronization offset is t.

The durations of the active and idle periods before and after the change of the channel status are independent, so we can write:

$$\begin{aligned} &P\{\hat{I}^{(1)}_R,\hat{I}^{(2)}_R|A^{(1)}_{\text{XY}},I^{(2)},z,t\} = \\ &= P\{\hat{I}^{(1)}_R|A^{(1)}_{\text{XY}},I^{(2)},z,t\}\cdot P\{\hat{I}^{(2)}_R|A^{(1)}_{\text{XY}},I^{(2)},z,t\}, \end{aligned}$$

$$P\{\mathcal{T}|\hat{I}_T^{(1)},\hat{I}_T^{(2)}\} = P\{\mathcal{T}|I^{(1)},I^{(2)}\}P\{I^{(1)},I^{(2)}|\hat{I}_T^{(1)},\hat{I}_T^{(2)}\} + \iint_{\mathcal{XY}} P\{\mathcal{T}|A_{\text{XY}}^{(1)}(x,y),I^{(2)}\}P\{A_{\text{XY}}^{(1)}(x,y),I^{(2)}|\hat{I}_T^{(1)},\hat{I}_T^{(2)}\}dxdy$$
$$+ \iint_{x,y\geq R_I(r)} P\{\mathcal{T}|I^{(1)},A_{\text{XY}}^{(2)}(x,y)\}P\{I^{(1)},A_{\text{XY}}^{(2)}(x,y)|\hat{I}_T^{(1)},\hat{I}_T^{(2)}\}dxdy \quad (42)$$
$$+ \iint_{\mathcal{XY}}\iint_{x_2,y_2\geq R_I(r)} P\{\mathcal{T}|A_{\text{XY}}^{(1)}(x_1,y_1),A_{\text{XY}}^{(2)}(x_2,y_2)\}P\{A_{\text{XY}}^{(1)}(x_1,y_1),A_{\text{XY}}^{(2)}(x_2,y_2)|\hat{I}_T^{(1)},\hat{I}_T^{(2)}\}dx_1dy_1dx_2dy_2$$

where:

$$P\{\hat{I}_R^{(2)}|A_{\text{XY}}^{(1)},I^{(2)},z,t\} = \begin{cases} p_{\text{MD}}(y), & z \geq t_{\text{gap}} - t, \\ 1 - p_{\text{FA}}, & \text{otherwise}, \end{cases}$$

and

$$P\{\hat{I}_R^{(1)}|A_{\text{XY}}^{(1)},I^{(2)},z,t\} \approx \frac{(1-p_{\text{FA}})\overline{F}_A(t+z)+p_{\text{MD}}(y)F_A(t+z)}{\overline{F}_A(z)},$$

where with the approximation we ignore the probability of the unlikely event of having an extremely short back-off period between the TR and RR's first sensing measurement. Finally, the probability of handshake is calculated as:

$$P\{\mathcal{T}|A_{\text{XY}}^{(1)}(x,y),I^{(2)}\} = \int_0^{t_{\text{gap}}} P\{\mathcal{T}|A_{\text{XY}}^{(1)}(x,y),I^{(2)},z\}dz, \quad (44)$$

where the conditional probability reduces to the product:

$$P\{\mathcal{T}|A_{\text{XY}}^{(1)}(x,y),I^{(2)},z\} = g(z)\cdot\overline{F}_{R_F|A_{\text{XY}}^{(1)},I^{(2)},z}^{(\text{TR,RR})}(t_{\text{hs}}).$$

The above conditional interference-free distribution, $\overline{F}_{R_F|A_{\text{XY}}^{(1)},I^{(2)},z}^{(\text{TR,RR})}(.)$ is calculated from (29), by substituting $f_{R_f|A_{\text{XY}}^{(1)},I^{(2)}}(t)$ with

$$f_{R_f|A_{\text{XY}}^{(1)},I^{(2)},z}(t) = \frac{1}{F_{R_A}(t_{\text{gap}})}f_{R_A}(z)\frac{f_I(t+t_{\text{gap}}-z)}{\overline{F}_I(t_{\text{gap}}-z)}.$$

We skip the derivations for the remaining channel status cases as the calculation methodology is similar.

5) Successful packet transmission: Finally, let us express the probability of successful packet transmission, now conditioned on the success of the handshake (Fig. 4(b)).

We update all $(S^{(1)},S^{(2)})$, through Bayesian inference:

$$P\{S^{(1)},S^{(2)}|\mathcal{T}\} = P\{S^{(1)},S^{(2)}|\mathcal{T},\hat{I}_T^{(1)},\hat{I}_T^{(2)}\} =$$
$$= \frac{P\{\mathcal{T}|S^{(1)},S^{(2)},\hat{I}_T^{(1)},\hat{I}_T^{(2)}\}P\{S^{(1)}S^{(2)}|\hat{I}_T^{(1)},\hat{I}_T^{(2)}\}}{P\{\mathcal{T}|\hat{I}_T^{(1)},\hat{I}_T^{(2)}\}} = \quad (45)$$
$$= \frac{P\{\mathcal{T}|S^{(1)},S^{(2)}\}P\{S^{(1)}S^{(2)}|\hat{I}_T^{(1)},\hat{I}_T^{(2)}\}}{P\{\mathcal{T}|\hat{I}_T^{(1)},\hat{I}_T^{(2)}\}},$$

where $P\{\mathcal{T}|\hat{I}_T^{(1)},\hat{I}_T^{(2)}\}$ is defined in (42), the terms $P\{\mathcal{T}|S^{(1)},S^{(2)}\}$ are derived in the previous Section and $P\{S^{(1)},S^{(2)}|\hat{I}_T^{(1)},\hat{I}_T^{(2)}\}$ is derived from (16).

Similarly, we update the total remaining interference-free time, T_{R_F}, with respect to the total length of the handshake time, including the synchronization delay, $t_{\text{hs}}^T = t_{\text{hs}} + t_{\text{SYNC}}$, as it is measured by the TR node:

$$\overline{F}_{R_F|(S^{(1)},S^{(2)}),\mathcal{T}}(t) =$$
$$= P\{T_{R_F} \geq t + t_{\text{hs}}^T | T_{R_F}^{(\text{TR,RR})} \geq t_{\text{hs}}^T\} =$$
$$= \frac{P\{T_{R_F}\geq t+t_{\text{hs}}^T, T_{R_F}^{(\text{TR,RR})}\geq t_{\text{hs}}^T\}}{P\{T_{R_F}^{(\text{TR,RR})}\geq t_{\text{hs}}^T\}} \approx \frac{\overline{F}_{R_F|(S^{(1)},S^{(2)})}(t+t_{\text{hs}}^T)}{\overline{F}_{R_F|(S^{(1)},S^{(2)})}^{(\text{TR,RR})}(t_{\text{hs}}^T)}, \quad (46)$$

where the respective density functions are given in (28) and (29), and the approximation is valid due to the relatively short handshake time with respect to the WLAN spectrum duty cycle.

Finally, from (42) and (46) we express the probability that a packet of transmission duration t will be successfully transmitted as:

$$P\{\text{transmission success}|\mathcal{T}\} =$$
$$= \sum \overline{F}_{R_F|(S^{(1)},S^{(2)}),\mathcal{T}}(t)P\{S^{(1)},S^{(2)}|\mathcal{T},\hat{I}_T^{(1)},\hat{I}_T^{(2)}\}, \quad (47)$$

where the summation is over all possible channel status $S^{(1)},S^{(2)}$.

C. COG-MAC performance over a shadowing channel model

This Section presents the required modifications on the analytic model of COG-MAC performance in order to derive the probability of successful transmission using a channel model that is extended with shadowing-based attenuation. In the following we describe the required channel model modifications and we revise the derivation steps presented in the above Section to account for the channel shadowing.

1) Shadowing model: The model that describes the signal attenuation over a wireless link is enhanced with a log-normally distributed shadowing gain. That is, the received signal power at distance d from a WLAN active source is given as

$$P_{Rx}(d) \triangleq P_{Rx}(d,\zeta) = P_{\text{WLAN}}P_{L_0}d^{-\eta}10^{\zeta/10} \quad (48)$$

where Z is a zero-mean Gaussian variable with standard deviation σ_{sh}, that is

$$f_Z(\zeta) = \frac{1}{\sigma_{\text{sh}}\sqrt{2\pi}}e^{-\frac{\zeta^2}{2\sigma_{\text{sh}}^2}}$$

while the other parameters and factors have been explained in Section III. (48) is, additionally, used to derive the received power on the TR-RR link. We assume that the shadowing gains of the existing WSN communication or interference links have independent realizations. Considering the interference model of Fig. 2 we denote by $Z_T, Z_R, Z_{\text{T-R}}$ the shadowing gains of the corresponding links, that is, between the WLAN source and the TR and RR nodes, and over the TR-RR link, respectively.

As a result, the instantaneous interference radius at the TR and RR nodes with respect to the shadowing realizations will be given as follows:

$$R_{\mathcal{I}}^{\text{TR}}(r,\zeta_{\text{SINR}},\eta,P_{\text{WSN}},P_{\text{WLAN}}) \triangleq$$
$$\triangleq R_{\mathcal{I}}^{\text{TR}}(r,\zeta_{\text{SINR}},\eta,P_{\text{WSN}}(\zeta_{\text{T-R}}),P_{\text{WLAN}}(\zeta_{\text{T}})) = \quad (49)$$
$$= \sqrt[\eta]{\frac{\zeta_{\text{SINR}}P_{\text{WLAN}}P_{L_0}10^{\zeta_{\text{T}}/10}}{P_{\text{WSN}}P_{L_0}r^{-\eta}10^{\zeta_{\text{T-R}}/10}-\zeta_{\text{SINR}}\sigma_N^2}},$$

$$R_{\mathcal{I}}^{\text{RR}}(r,\zeta_{\text{SINR}},\eta,P_{\text{WSN}},P_{\text{WLAN}}) \triangleq$$
$$\triangleq R_{\mathcal{I}}^{\text{RR}}(r,\zeta_{\text{SINR}},\eta,P_{\text{WSN}}(\zeta_{\text{T-R}}),P_{\text{WLAN}}(\zeta_{\text{R}})) = \quad (50)$$
$$= \sqrt[\eta]{\frac{\zeta_{\text{SINR}}P_{\text{WLAN}}P_{L_0}10^{\zeta_{\text{R}}/10}}{P_{\text{WSN}}P_{L_0}r^{-\eta}10^{\zeta_{\text{T-R}}/10}-\zeta_{\text{SINR}}\sigma_N^2}},$$

In addition, we make the simplifying assumption that the shadowing realizations are constant within the short period of a WSN duty cycle. Consequently, the performance of both the short-period channel sensing and of the WSN transmission depends on the instantaneous shadowing gains. While the false alarm proability is unaffected, the missed detection probability is now given by integrating Eq. (3) over the shadowing density:

$$p_{\text{MD}}(t_s,d;\gamma(p_{\text{FA}})) \triangleq \int_0^\infty p_{\text{MD}}(\zeta)f_Z(\zeta)d\zeta =$$
$$= 1-\int_0^\infty \mathcal{Q}\left(\frac{\gamma(p_{\text{FA}})-(\sigma_N^2+P_{Rx}(d,\zeta))}{\sigma_N^2\sqrt{2/(f_s t_s)}}\right)f_Z(\zeta)d\zeta, \quad (51)$$

where $Z\in\{Z_{\text{T}},Z_{\text{R}}\}$. Shadowing gains, additionally, affect the radius of observable WLAN occupancy, which in accordance with Eq. (4) will be given by

$$R_{\text{CCA}} \triangleq R_{\text{CCA}}(\psi) = \left(\frac{\psi-\sigma_N^2}{\mathbb{E}[P_{\text{WLAN}}]P_{L_0}}\right)^{-1/\eta}, \quad (52)$$

where the expected signal power will be

$$\mathbb{E}[P_{\text{WLAN}}] = P_{\text{WLAN}}\cdot 10^{\sigma_{\text{sh}}^2/2}.$$

(52) is used to calculate both observable radii, namely, $R_{\text{CCA}},\hat{R}_{\text{CCA}}$.

2) Spatial distribution of WLAN interfering sources: The a-priori spatial distributions, $f_X(x)$, $f_{Y|X}(x,y)$, of the WLAN interfering transmitters inside the AP area do not depend on shadowing, as they consider no sensing information and can be calcuated with basic geometry, as discussed in Section VI. Shadowing, however, affects the a-priori spatial distributions, $p_{A_X}(x)$, $p_{A_{Y|X}}(x,y)$, which are defined in (12)–(14), since the observable load is no longer restricted inside a fixed CCA area. Under shadowing, R_{CCA} and $\hat{R}_{\text{CCA}}^T$ are not any more well-defined. In the following we show how $p_{A_X}(x)$ can be derived, assuming an observable load p_{CCA}^T at the TR node. We have the following decomposition:

$$p_{A_{\text{X}}}(x) \triangleq P\{\text{WLAN at dist. } x\} =$$
$$= P\{\text{WLAN at dist. } x|\text{belongs to det. load}\}\cdot$$
$$\cdot P\{\text{belongs to det. load}\}+ \quad (53)$$
$$P\{\text{WLAN at dist. } x|\text{belongs to non-det. load}\}\cdot$$
$$\cdot P\{\text{belongs to non-det. load}\}$$

where, clearly, $P\{\text{belongs to non-det. load}\}=1-p_{\text{CCA}}^T$, and $P\{\text{belongs to det. load}\}=p_{\text{CCA}}^T$. Using Bayesian inference, we derive the conditional probabilities in (53) as follows:

$$P\{\text{WLAN at dist. } x|\text{belongs to det. load}\} =$$
$$= 2x\,(1-p_{\text{MD}}(x))\,/\int_{\mathcal{X}} 2u\,(1-p_{\text{MD}}(u))\,du, \quad (54)$$

$$P\{\text{WLAN at dist. } x|\text{belongs to det. load}\} =$$
$$= 2x\;p_{\text{MD}}(x)/\int_{\mathcal{X}} 2u\;p_{\text{MD}}(u)du. \quad (55)$$

In the absence of shadowing, $p_{\text{MD}}(u)$ is binary, and (53) reduces to (12). The rest of the derivations are similar. (53) reflects that additional uncertainty in the a-priori information about the possible locations of the WLAN interferers, as a result of channel shadowing.

3) Bayesian inference of channel status: The posterior distribution of WLAN channel status given the idle measurements at the transmitting sensor, $P\{S^{(1)},S^{(2)}|\hat{I}_T^{(1)},\hat{I}_T^{(1)}\}$, depends on the probability of missed detection (Eq. (51)), which is now a function of the shadowing gains on the interfering links. However, as the dependence is only through p_{md}, the posterior channel status can still be given by Eq. (17)–Eq. (19) and Eq. (24)–Eq. (27).

4) Conditional remaining interference-free time: Conditioned on the channel status $\left(S^{(1)},S^{(2)}\right)\in\mathcal{S}$ the remaining times T_{R_f} (Fig. 5), whose densities are defined in Eq. (32) – Eq. (36), do not depend on the shadowing gains of the links.

However, this does not hold for the total interference-free times, $T_{R_F},T_{R_F}^{\text{TR-RR}}$ defined in Eq. (28) – Eq. (29), as they depend on the probability that the following active WLAN active period will interfere with the WSN communication, $p_{\mathcal{IN}},p_{\mathcal{IN}}^{(\text{TR,RR})}$ (Eq. (30), Eq. (31)), which are functions of the shadowning gains. To this end, we extend $p_{\mathcal{IN}}$ as a function of the shadowing gains to $p_{\mathcal{IN}}(\zeta_{\text{R}},\zeta_{\text{T-R}})$ by substituting $R_{\mathcal{I}}(r)$ in (30) with the expression in (50). Similarly, we extend $p_{\mathcal{IN}}^{\text{TR-RR}}$ as a function of the shadowing gains $\zeta_{\text{T}},\zeta_{\text{R}},\zeta_{\text{T-R}}$, that is, $p_{\mathcal{IN}}^{\text{TR-RR}}(\zeta_{\text{T}},\zeta_{\text{R}},\zeta_{\text{T-R}})$ by substituting $R_{\mathcal{I}}(r)$ in (31) with the expression in (49). Finally, we average over the shadowing gains of the interfering links, that is

$$p_{\mathcal{IN}}(\zeta_{\text{T-R}}) = \int_0^\infty p_{\mathcal{IN}}(\zeta_{\text{R}},\zeta_{\text{T-R}})f_{Z_{\text{R}}}d\zeta_{\text{R}} \quad (56)$$

$$p_{\mathcal{IN}}^{\text{TR-RR}}(\zeta_{\text{T-R}}) = \int_0^\infty\int_0^\infty p_{\mathcal{IN}}(\zeta_{\text{T}},\zeta_{\text{R}},\zeta_{\text{T-R}})f_{Z_{\text{T}}}(\zeta_{\text{T}})f_{Z_{\text{R}}}(\zeta_{\text{R}})d\zeta_{\text{T}}d\zeta_{\text{R}}. \quad (57)$$

$F_{T_R|S^{(1)},S^{(2)}},F_{T_R|S^{(1)},S^{(2)}}^{\text{TR-RR}}$ are, then, functions of $\zeta_{\text{T-R}}$.

5) TR-RR handshake success: The calculation of the probability of successful handshake depends on the shadowing gains through both the missed detection probability and the remaining interference-free time. In particular, the expression in Eq. (38) must be integrated over $\zeta_{\text{T-R}}$ applying the expression in (57) on the total remaining interference-free time. The expression in Eq. (39) must, instead, be integrated over $\zeta_{\text{R}},\zeta_{\text{T-R}}$, and extend $p_{\text{MD}}(y)$ to $p_{\text{MD}}(y,\zeta_{\text{R}})$ (Eq. (51)).

For the cases when a WLAN source is active at the point of the second measurement (Eq. (40), Eq. (41)), the remaining interference-free time and missed detection events are coupled, so the events of successful handshake are integrated over all shadowing gains, $\zeta_{\text{T}},\zeta_{\text{R}},\zeta_{\text{T-R}}$, and must, additionally, be multiplied by $p_{\mathcal{IN}}^{\text{TR-RR}}(\zeta_{\text{T}},\zeta_{\text{R}},\zeta_{\text{T-R}})$, i.e. the probability that the active WLAN source at the point of the second channel measurement does not interfere with the TR-RR handshake process. We, finally, apply (42) to determine the probability of handshake success.

6) Successful packet transmission: Given the event of successful handshake, the posterior probabilities of channel status are calculated similar to (45) but, additionally, as functions of the shadowing gain over the TR-RR link, $\zeta_{\text{TR-RR}}$. The updates of the total remainining interference-free time are done as in

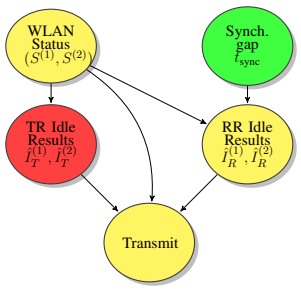

Fig. 6. Bayesian network, representing the causal relations of events during packet transmission without RTS/CTS handshake.

(46) where $p_{\mathcal{IN}}(\zeta_{\text{T-R}})$ is extended to $p_{\mathcal{IN}}^{\text{TR-RR}}(\zeta_{\text{T-R}})$ as discussed above. In order to derive the probability of successful packet transmission with respect to packet transmission time and next-hop distance, we must, finally, integrate (47) over the shadowing gain $\zeta_{\text{T-R}}$.

D. COG-MAG modeling without the RTS/CTS handshake mechanism

In the absense of the RTS/CTS handshake, a packet transmission is attempted by the TR directly after the back-off period (Fig. 3). As a result, the probability of successful packet reception depends only on the conditional interference-free time seen by the TR node, given the pair of idle measurements. The situation is illustrated in Fig. 6. The analytic model modifications for the COG-MAC probability of successful packet tranmission without the RTS/CTS mechanism have been given in detail in our earlier work [27], Eq.(13)-(15).

VII. CSMA & RAND Modeling

We present here the analytic models for the legacy 802.15.4-compliant (CSMA) and Random Access (RAND) MAC protocols, that are required for the performance evaluation in Section VIII. Similarly to Section VI we, first, derive the probability of successful transmission with respect to the TR-RR distance and to the packet length. We then proceed with the calculation of the energy consumption considering the repeated TR-RR handshake and transmission attempts that are required for each transmitted packet. Based on the derived energy consumption models we are able to formulate the optimization problems for CSMA and RAND similarly to (11) and derive for each protocol the optimal packet size and transmission distance that minimize the energy cost of transmitting one bit ofinformation under the given WLAN channel occupancy conditions.

A. CSMA: Probability of successful transmission

The process of deriving the probability of successful transmission is similar to the one for COG-MAC, described in VI-B with the exception of having a single channel measurement at each duty-cycle. In this Section we describe in detail the required changes in the derivation steps as a result of the single channel energy measurement. We can omit the superscript (i) for the events of channel status, S, and node idle measurements, $\hat{I}_T, \hat{I}_R$, due to the single measurement instant. The Bayesian networks representing the causal relations in the node handshake and packet transmission process are given in Fig. 7.

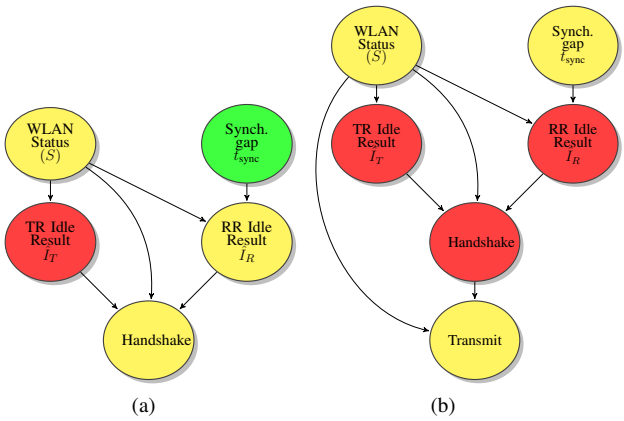

Fig. 7. Bayesian networks representing the causal relations in the handshake, (a), and transmission process, (b), for the CSMA (single measurement) case. With red color are the observed (instantiated) variables, that affect the variables in yellow, but not the ones in green.

The derivation of the spatial distribution of the WLAN interfering sources (Step 1) is identical to the COG-MAC case (Section VI-B1). Applying Bayesian formulation we derive in Step 2 the posterior distribution of the channel status conditioned on the single TR idle measurement, $P\{S|\hat{I}_T\}$, $S = I, A_{\text{XY}}$, using Eq. (16)–(19) (Section VI-B2), omitting the time index.

In Step 3 we calculate the total interference-free time densities, $f_{R_F|S}(t), f_{R_F|S}^{(\text{TR,RR})}(t)$, similarly to $f_{R_F|S^{(1)},S^{(2)}}(t), f_{R_F|S^{(1)},S^{(2)}}^{(\text{TR,RR})}(t)$ in Section VI-B3 (Eq. (28)–(29)):

$$f_{R_F|S}(t) = \mathcal{L}^{-1}\left\{\frac{p_{\mathcal{IN}} f_{R_f|S}^*(s)}{1-(1-p_{\mathcal{IN}})f_I^*(s)f_A^*(s)}\right\}, \quad (58)$$

$$f_{R_F|S}^{(\text{TR,RR})}(t) = \mathcal{L}^{-1}\left\{\frac{p_{\mathcal{IN}}^{(\text{TR,RR})} f_{R_f|S}^*(s)}{1-(1-p_{\mathcal{IN}}^{(\text{TR,RR})})f_I^*(s)f_A^*(s)}\right\}, \quad (59)$$

The probabilities $p_{\mathcal{IN}}, p_{\mathcal{IN}}^{(\text{TR,RR})}$ are calculated as in Eq. (30)–(31), while the density $f_{R_f|S}(t)$ is calculated as follows:

For $S = I$ (Fig. 8(a)) we simply have $f_{R_f|I}(t) = f_{R_I}(t)$, where $f_{R_I}(t)$ denotes the density of the remaining idle time, T_{R_I} defined in Section VI-B2, while for $S = A_{\text{XY}}$ (Fig. 8(b)) we have $f_{R_F|A_{\text{XY}}}(t) = f_{R_A}(t) * f_I(t)$.

The process of calculating the probability of successful handshake (Step 4), in the case of perfect synchronization, resembles the one for COG-MAC, where (37) is reduced to:

$$P\{\mathcal{T}|S\} = P\{\hat{I}_R|S\}\overline{F}_{R_F|S}^{(\text{TR,RR})}(t_{\text{hs}}). \quad (60)$$

and the set of Equations (38)–(41) is reduced to:

$$P\{\mathcal{T}|I\} = (1-p_{\text{FA}})\overline{F}_{R_F|I}^{(\text{TR,RR})}(t_{\text{hs}}), \quad (61)$$

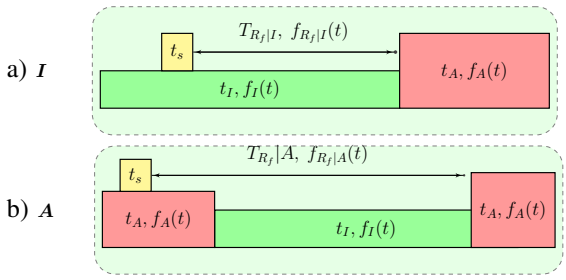

Fig. 8. Diagram for the calculation of remaining time densities for the CSMA modeling.

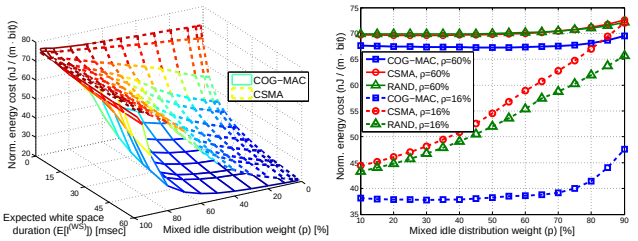

(a) (b)

Fig. 9. (a) Comparison of Cognitive and CSMA-based MAC over p and σ, and (b) normalized energy cost with respect to p for fixed WLAN Load ($\rho = 16\%$ and 60%)

$$P\{\mathcal{T}|A_{\rm XY}(x,y)\} = \\ = p_{\rm MD}(y)\overline{F}^{\rm (TR,RR)}_{R_F|A_{\rm XY}}(t_{\rm hs}),\ x\in\mathcal{X}, y\geq R_I(r). \quad (62)$$

Finally, the probability of handshake, $P\{\mathcal{T}|\hat{I}_T\}$, is calculated over all possible cases, similarly to (42):

$$P\{\mathcal{T}|\hat{I}_T\} = P\{\mathcal{T}|I\}P\{I|\hat{I}_T\}+ \\ +\int\int_{x,y\geq R_I(r)} P\{\mathcal{T}|A_{\rm XY}(x,y)\}P\{A_{\rm XY}(x,y)|\hat{I}_T\}dxdy \quad (63)$$

We consider now the case of imperfect TR-RR synchronization. Due to the synchronization gap the TR and the RR may sense at different channel status. Consider, first that $S = A_{\rm XY}$. As in Section VI-B we aim at computing the probability of the event $\hat{I}_R|A_{\rm XY}, z$ of an idle RR measurement, when the channel status transition occurs at time $t_{R_A} = z$ after the TR measurement (Fig. 8(b)). (43) is reduced to:

$$g(z) \triangleq P\{\hat{I}_R|A_{\rm XY},z\} = \int_0^{t^{\rm max}_{\rm sync}} P\{\hat{I}_R|A_{\rm XY},z,t\}f_{\rm sync}(t)dt, \quad (64)$$

where we have:

$$P\{\hat{I}_R|A_{\rm XY},z,t\} = \begin{cases} p_{\rm MD}(y), & z\geq t, \\ 1-p_{\rm FA}, & \text{otherwise.}\end{cases}$$

The probability of handshake is, now, calculated by reducing (45) to

$$P\{\mathcal{T}|A_{\rm XY}(x,y)\} = \int_0^{t_{\rm gap}} g(z)\cdot\overline{F}^{\rm (TR,RR)}_{R_F|A_{\rm XY},z}(t_{\rm hs})dz, \quad (65)$$

The calculation of the handshake probability when $S = I$ is skipped as it follows the same methodology.

Finally, let us express the probability of successful packet transmission, now conditioned on the success of the handshake (Fig. 7(b)). The probability of the spectrum status is updated through Bayesian inference similarly to (45):

$$P\{S|\mathcal{T}\} = P\{S|\mathcal{T},\hat{I}_T\} = \frac{P\{\mathcal{T}|S,\hat{I}_T\}P\{S|\hat{I}_T\}}{P\{\mathcal{T}|\hat{I}_T\}} = \\ = \frac{P\{\mathcal{T}|S\}P\{S|\hat{I}_T\}}{P\{\mathcal{T}|\hat{I}_T\}}, \quad (66)$$

whose terms have all been calculated above. The Equations (46)–(47) are, finally, reduced to:

$$\overline{F}_{R_F|S,\mathcal{T}}(t) = \\ = P\{T_{R_F}\geq t+t^T_{\rm hs}|T^{\rm (TR,RR)}_{R_F}\geq t^T_{\rm hs}\} = \\ = \frac{P\{T_{R_F}\geq t+t^T_{\rm hs}, T^{\rm (TR,RR)}_{R_F}\geq t^T_{\rm hs}\}}{P\{T^{\rm (TR,RR)}_{R_F}\geq t^T_{\rm hs}\}} \approx \frac{\overline{F}_{R_F|S}(t+t^T_{\rm hs})}{\overline{F}^{\rm (TR,RR)}_{R_F|S}(t^T_{\rm hs})}, \quad (67)$$

$$P\{\text{transmission success}|\mathcal{T}\} = \\ = \textstyle\sum_{S=A_{\rm XY},I}\overline{F}_{R_F|S,\mathcal{T}}(t)P\{S|\mathcal{T},\hat{I}_T\}, \quad (68)$$

The derivation of energy-optimal receiver distance, r^*, and packet size, t^*, resembles the one for COG-MAC in Section VI-A.

B. RAND: Probability of successful transmission

Under the simplistic random access MAC the communicating nodes do not perform carrier sense and RTS/CTS handshake. Therefore, the probability of successful transmission of a packet with transmission time t at a receiving node at distance r equals the probability that the total interference-free time, T_{R_F}, exceeds the transmission time, t:

$$P\{\text{transmission success}\}(r,t) = \\ = p_I P\{T_{R_F|I}\geq t\} + \int\int_{x,y\geq R_I(r)} p_A p_{A_{\rm XY}}(x,y)\cdot \\ \cdot P\{T_{R_F}|A_{\rm XY}(x,y)\geq t\}dxdy \quad (69)$$

Similarly to the CSMA case, the total interference-free time densities are conditioned on the spectrum status, S, at the beginning of the duty-cycle, and, therefore, have the form of Eq. (58)–(59). The same applies for the densities $f_{R|S}(t),\ S\in\{A,I\}$. The derivation of the spatial density $p_{A_{\rm XY}}(x,y)$ follows the procedure in Section VI-B.

Under the RAND scheme the expected energy cost of successful packet delivery does not include the energy cost for TR-RR handshake, and, therefore, (10) is reduced to:

$$E_{\rm trans}(r,t) = \frac{P^{\rm WSN}_{\rm ON}\cdot t}{P\{\text{transmission success}(r,t)\}}. \quad (70)$$

The derivation of energy-optimal receiver distance and packet size is conducted as in Section VI-A, substituting (70) in the optimization problem (11).

TABLE I
PARAMETER SETUP FOR THE PERFORMANCE EVALUATION

Channel Model	
Path-Loss Exponent (η)	3.0
Ref. Distance attenuation (P_{L_0})	Isotropic $(\lambda/(4\pi)))^2$
Noise Power (σ_N^2)	-174 dB/Hz
WLAN Properties & Modeling	
Bandwidth (B_{WLAN})	22MHz (802.11x Channel)
Tx-Power	18dBm (22MHz Channel)
Tx-Power inside WSN band (P_{WLAN})	12dB
Max. back-off period (α_{BK})	700μsec
Active period interval ($\alpha_{\text{ON}}, \beta_{\text{ON}}$)	(0.8msec, 1.5msec)
White space Pareto scale (ξ)	0.3095
WSN & CC2420 Properties	
Bandwidth (B_{WSN})	5MHz Zigbee Channel
Tx-Power (P_{WSN})	1dBm
Tx-Rate (R_{WSN})	250kbps
Header Length [Packet overhead] (L_0)	13 bytes
RTS/CTS Length	6 bytes
Minimum SINR (ζ_{SIR})	5dB
Receiver Sensitivity (ψ)	-100 dBm
RSSI Dynamic Range	100dB
Tx/Rx Power Consumption ($P_{\text{ON}}^{\text{WSN}}$)	55mW
Handshake Duration (t_{hs})	768μsec
Channel Sensing Model	
Sampling Frequency (f_s)	5MHz
Sensing Time (t_s)	16μsec
False Alarm Constraint (p_{FA})	10^{-2}

VIII. NUMERICAL PERFORMANCE EVALUATION

We evaluate the performance of COG-MAC, based on the analytic model in Section VI, by comparing it to duty-cycled, non-cognitive WSN MAC schemes. In particular, we consider an ALOHA-type Random Access MAC (RAND), where sensors transmit at the beginning of the duty-cycle without any channel sensing before transmission, and a standard 802.15.4-compliant carrier-sense (CSMA) MAC scheme, where WSN nodes perform the standard channel sensing and RTS/CTS handshake. The analytic models for RAND and CSMA are similar to that of COG-MAC and are not presented here due to space limitation. Interested readers can find them in [33]. For all the three schemes we consider the normalized energy cost metric under optimized transmission distance and packet size as defined by (11). The default parameters of our reference evaluation scenario are listed in Table I.

A. Comparison with RAND & CSMA schemes

Fig. 9(a) compares the normalized energy cost of COG-MAC and CSMA with respect to the parameter p, the percentage of short WLAN back-off intervals, and $E\left[I^{(\text{WS})}\right] = \frac{\sigma}{1-\xi}$, the average length of white spaces, controlled by the shape parameter σ of the generalized Pareto distribution. We set the observable load at the receiving sensor at $p_{\text{CCA}}^R = 0.5$. To consider random transmitter location we randomize $\hat{p}_{\text{CCA}}^T$, following a normalized binomial distribution, in $[0, p_{\text{CCA}}^R]$. In general, increasing p or decreasing $E\left[I^{(\text{WS})}\right]$ increases the load and consequently the normalized energy consumption for both protocols. Fig. 9(a), however, shows that COG-MAC significantly outperforms CSMA. In Fig. 9(b) we keep the load constant at $\rho = 16\%$ and 60%, and increase the percentage of the back-off periods p. Even in this case COG-MAC shows better normalized energy consumption compared

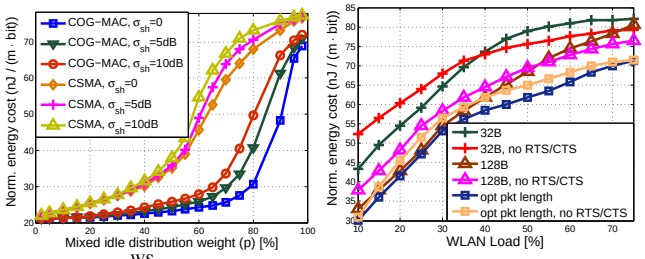

(a) $\bar{I}^{\text{WS}} = 60$ms (b) $p = 0.8$

Fig. 10. (a) COG-MAC – CSMA comparison with respect to the normalized energy cost under log-normal shadowing and (b) fixed packet lengths.

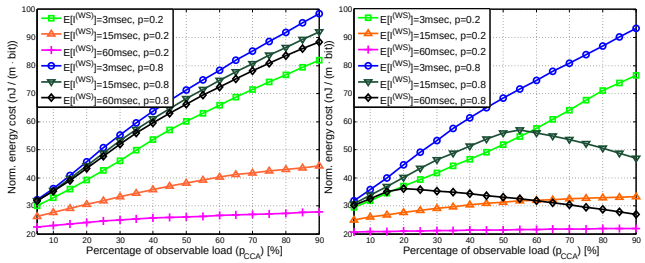

(a) CSMA (b) COG-MAC

Fig. 11. Normalized energy cost with respect to the percentage of the observable WLAN spectrum activity (p_{CCA}).

to both CSMA and RAND. The energy cost of COG-MAC is only marginally affected by the growing percentage of back-off periods. In contrast, RAND and CSMA, due to the fact that they have to optimize transmission parameters for the mixture idle time distribution, cannot provide energy efficient communication for a large range of p.

1) Impact of channel shadowing: Fig. 10(a) compares COG-MAC to CSMA under log-normal shadowing channel model and for various shadowing standard deviation (σ_{sh}) values. Shadowing on the wireless channel degrades the WSN communication energy efficiency as it adds uncertainty in both the WLAN spatio-temporal model estimation and the interference calculation, and the degradation is significant for COG-MAC at high WLAN load. Still, the large performance gap between the two solutions remains.

2) Impact of the RTS/CTS handshake mechanism: Fig. 10(b) compares the efficiency of COG-MAC with and without RTS/CTS exchange under increasing WLAN channel load – decreasing average white-spaces duration – and for fixed and optimized WSN packet lengths. We observe that RTS/CTS is always beneficial under optimized packet lengths. For fixed packet sizes the effect of RTS/CTS handshake depends on the WLAN load. Under high load values, that is, under short expected white-space durations, the increased performance due to efficient white-space discovery is limited, thus, it does not compensate for the additional overhead of the RTS/CTS mechanism.

3) Impact of the receiver observable load: Let us now investigate the effect of the observable load p_{CCA}^R on energy efficiency. Fig. 11 compares the CSMA and COG-MAC normalized energy cost as a function of p_{CCA}^R and for different p and $E\left[I^{(\text{WS})}\right]$ values. For the CSMA scheme (Fig. 11(a))

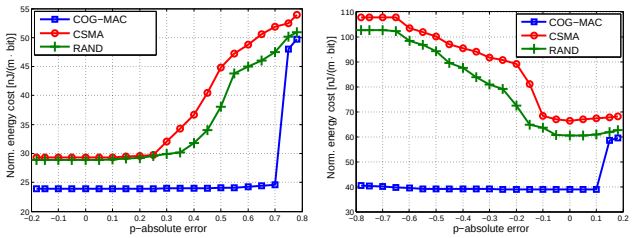

(a) $p = 0.2$ (b) $p = 0.8$

Fig. 12. Normalized energy cost with respect to the absolute of error in p-estimation, $[\hat{p} - p]$. $E\left[I^{(\mathrm{WS})}\right] = 36$msec ($\sigma = 0.025$).

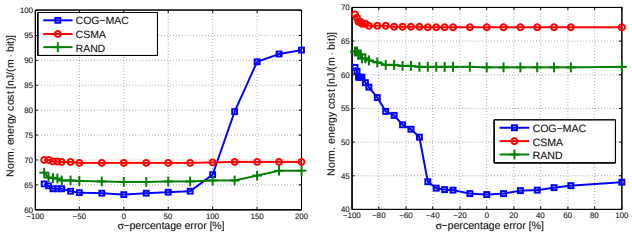

(a) $\sigma = 5 \cdot 10^{-3}$ (7msec) (b) $\sigma = 2 \cdot 10^{-2}$ (30msec)

Fig. 13. Normalized energy cost with respect to the percentage of error in σ-estimation, $[(\hat{\sigma} - \sigma)/\sigma]$. $p = 80\%$.

the energy cost increases monotonically with the observable load, since the interference-free time decreases. We can see similar trends for COG-MAC for low p values in Fig. 11(b). On the contrary, at high p value the COG-MAC energy cost decreases at high p^R_{CCA}, because in these scenarios COG-MAC can efficiently filter the short back-off periods. As a result, COG-MAC can provide energy efficient communication despite the limited sensing range, and can decrease the energy cost with up to 66% compared to CSMA.

4) Sensitivity to the model parameters: COG-MAC may not be able to use optimal packet size and transmission distance due to imperfect WLAN Local View parameter estimation and due to the limited number of options that can be stored in the look-up table in the sensor memory. Therefore we evaluate the effect of estimation errors, considering the p and σ values. (The results for the other Local View parameters are similar.) Fig. 12 shows the effect of the imperfect estimation of p, for low and high p values. We can see that COG-MAC is not sensitive to estimation error, unless p is heavily overestimated, since the dual sensing filters out the back-off periods. On the contrary, CSMA and RAND need to taking the short back-off periods into account for the optimization, and therefore the imperfect estimation of p deteriorates their performance.

Fig. 13 depicts the sensitivity of the performance on the estimation of σ, the shape parameter of the white space distribution. For the considered scenario CSMA and RAND are not sensitive to estimation errors due to the high p value that makes the estimation of the actual WLAN white spaces less important. COG-MAC, however, transmits in the white spaces only, and therefore the over- and underestimation of σ leads to increased energy consumption. Still up to 50% error in estimating σ does not have significant effect on the energy cost. Based on [34], this level of accuracy can be achieved by considering 100-1000 idle period samples. This in turn leads

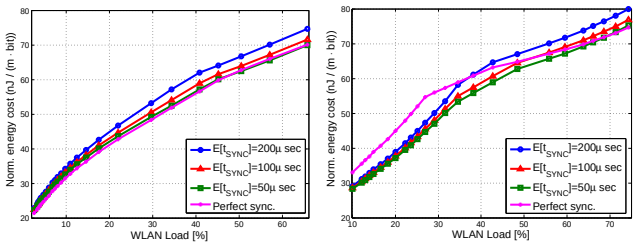

(a) $p = 20\%$ (b) $p = 80\%$

Fig. 14. Normalized communication energy cost with respect to increasing WLAN load (decreasing expected white-space duration), for different average synchronization offsets. $E\left[I^{(\mathrm{WS})}\right] = 60$msec.

to an estimation time in the order of 1-10 seconds, depending on the average lengths of the idle periods. The low sensitivity to estimation errors allows even the use of look-up tables with low granularity. These confirm that the proposed approach with local channel estimation and parameter optimization based cognitive access is a viable solution for sensor networks.

B. The effect of loose synchronization

In Fig. 14 we evaluate the energy cost of COG-MAC considering the case of imperfect synchronization of the TR and RR duty cycles, based on the model in [33]. We consider synchronization gaps uniformly distributed in $(0, t^{\max}_{\mathrm{sync}})$, $E[t_{\mathrm{SYNC}}] = t^{\max}_{\mathrm{sync}}/2$. We show the effect of $E[t_{\mathrm{SYNC}}]$ on the normalized COG-MAC energy cost as a function of the WLAN load, for low and high p values. Since the shifted double sensing procedures require more time, synchronization gaps decrease the probability of successful handshake and reduce the interference-free time for packet transmission, and therefore can increase the energy cost, as demonstrated in Fig. 14(a). Fig. 14(b), however, shows that for high p values and low network load synchronization gaps may slightly improve protocol performance. The time-shift of the TR and RR sensing times increases the chance of detecting a WLAN transmission after undetected active period and back-off time, and consequently increases the probability that the transmission happens in WLAN white space. All in all, synchronization offsets in the order of 100μsec have only a slight impact on the protocol performance.

IX. A Simulation Study of COG-MAC

The model-based evaluation in Section VIII is subject to the following assumptions that we have introduced to simplify the modeling:

1) The WLAN sources are uniformly distributed around the sensors. The actual spatial distribution of WLAN sources differs from uniform due to edge effects and since the number of the sources in an AP area is limited and their mobility is low.
2) The consecutive handshake and packet transmission attempts in COG-MAC observe independent WLAN channel status. This assumption of statistical independence is valid as long as the duration of WSN duty-cycle is long

enough compared to the dynamics of the WLAN activity model.

To simplify the derived analytical expressions, we made two approximations in the model (presented in the supplementary material). In (37), to simplify the expression of handshake success probability, we introduce the approximation that WLAN sources must remain silent inside the interference areas of both the TR and RR nodes during handshake, which slightly underestimates the handshake success probability. Also, in (46), the approximation of the interference-free time after handshake becomes rough unless the average interference-free time is relatively long compared to the handshake period.

We present, here, a simulation study of COG-MAC, where the above assumptions and approximations are removed. The comparison between numerical and simulation results will show whether the considered approximations in favor of analytic tractability are valid. In addition, we evaluate the time-stability of the protocol, and discuss its performance in multihop networks.

A. Implementation and Simulation Scenario

We simulate the coexisting networks in the NS-Miracle framework [37]. For the WLAN nodes we use the already implemented 802.11b compliant protocol stack. For the WSN nodes we have implemented a customized Physical Layer module that includes the SINR threshold-based packet reception model, as described in Section III, along with the energy detection-based dual channel sensing and a Medium Access Control module that implements the state machine of COG-MAC. WSN packet losses trigger retransmissions, occurring at consecutive duty cycles with a default value of 50msec.

We consider a single WLAN AP area with a limited set of wireless terminals (WTs), operating in the high SNR regime. We inject WLAN traffic by generating a packet stream that creates a sequence of idle and active periods that follow the proposed parameterized Global View model, and assign the packets to the WTs and the AP independently at random. To simulate a practical case we allocate 50% of the injected packets to the AP, while the rest are assigned uniformly at the WTs. In the WSN we simulate the single hop communication of a TR-RR sensor pair, separated by the optimal transmission distance r, and transmitting packets of optimal size. We consider saturated buffer to minimize simulation time.

Each simulation experiment with a particular TR-RR distance, r, consists of 100 simulation runs, for each of which the TR is randomly placed on the circumference of the circle with radius r around the RR to achieve the randomization of $\hat{p}^T_{\text{CCA}}$ (Fig. 2); the results are, then, averaged over those 100 runs. Each simulation run terminates when the TR sensor completes the transmission of 500 packets, or, alternatively, when the simulation time exceeds 1000 seconds.

B. Model Validation

We aim at validating the derived analytic model of COG-MAC by comparing its numerically calculated energy efficiency in Section VIII with the resulting efficiency evaluated through simulations.

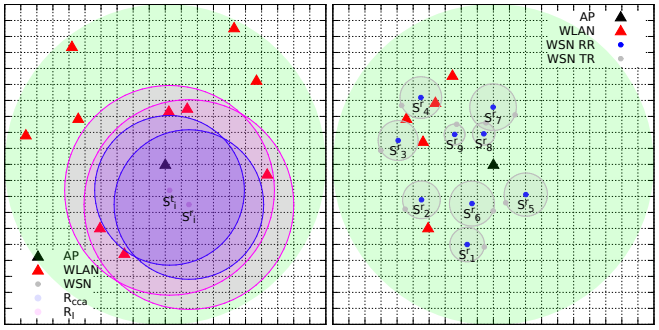

(a) (b)

Fig. 15. (a) An example of a topology realization for the model validation study where the detection and interference areas are illustrated for a single TR-RR communicating pair. (b) A topology realization with fixed AP, WT and RR locations. Receiving node s_i^R observes $i * 10\%$ of WLAN load.

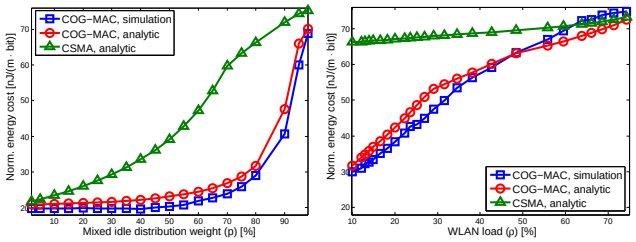

(a) $\bar{I}^{(\text{WS})} = 60$msec (b) $p = 0.8$

Fig. 16. Comparison between numerical and simulation results for COG-MAC under various p,σ parameterization sets.

We perform controlled experiments for a limited set of pairs $(p, E\left[I^{(\text{WS})}\right])$ as follows. For each experiment we first place a single RR sensor uniformly at random at a distance lower than R_{CCA} from the AP and deploy 10 WTs uniformly at random outside the $\mathcal{A}^R_{\text{CCA}}$. Thus the RR observes 50% of the WLAN traffic ($p^R_{\text{CCA}} = 0.5$). We determine the optimal distance r and the packet size for possible $\hat{p}^T_{\text{CCA}}$ values by the optimal solution of (11), and place the TR randomly in a valid position. Fig. 15(a) illustrates an example of a topology realization. To achieve statistical averages we randomize the location of the RR and the 10 deployed WTs for each simulation run within each experiment. The energy cost is calculated based on the number of the handshake and transmission attempts that each packet experiences.

In Fig. 16 we present comparative results for the normalized energy cost as it is predicted by the analytic model and as it is evaluated in our simulator. The comparison is done in Fig. 16(a) with respect to p and in Fig. 16(b) with respect to increasing WLAN load, ρ, by decreasing the expected white space durations. We observe in both figures a slight overestimation of the communication energy cost by the analytic model; the general conclusion, however, is that the model sufficiently captures the performance of the designed COG-MAC. The numerically evaluated performance of CSMA is also plotted for the sake of comparison.

Let us now evaluate the effect of the length of the WSN duty-cycle on COG-MAC performance, and thus the accuracy of the modeling assumption of independent WLAN channel status at the consecutive dual sensing events.

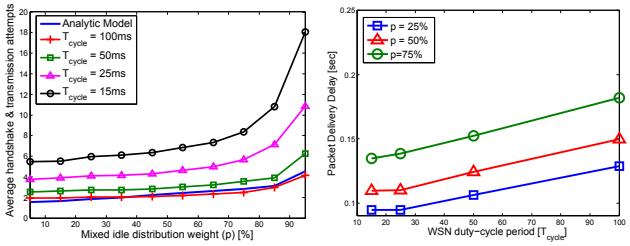

(a) (b)

Fig. 17. (a) Handshake and transmission attempts with respect to increasing percentage of back-off periods, parameterized by the WSN duty-cycle duration, (b) Packet delivery delay with respect to WSN duty cycle duration. Expected WLAN white space duration: $\bar{I}^{(\mathrm{WS})} = 36ms$.

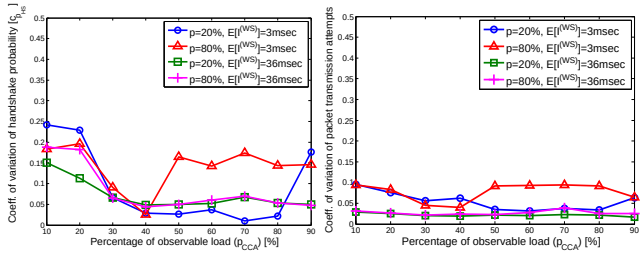

(a) (b)

Fig. 18. Coefficient of variation of (a) the number of handshake attempts and (b) the number of packet retransmissions under various WLAN observable traffic values.

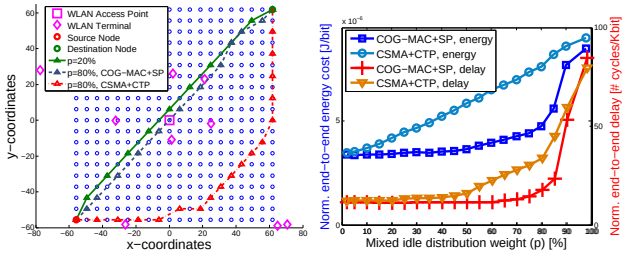

(a) (b)

Fig. 19. (a) Topology and transmission paths for COG-MAC and CSMA based cross-layer design schemes under different percentage of WLAN back-off periods. (b) Normalized end-to-end energy cost per bit and end-to-end delay with respect to increasing percentage of WLAN back-off periods. $\bar{I}^{(\mathrm{WS})} = 36ms$.

We consider the average per packet handshake and transmission attempts, and the average delay from the first handshake attempt to successful packet delivery, for duty-cycle periods from 15ms to 100ms. For the expected WLAN white space duration we choose a moderate value of 36msec, and tune p to change the WLAN load. In Fig. 17(a) we observe that as the WSN cycle duration increases above 50msec, the simulated performance matches closely the performance predicted by the analytic model, and for 100ms the performance difference is negligible, as the time between successive handshake or transmission attempts is long enough for COG-MAC to experience statistical independence. Similarly, Fig. 17(b) shows that the average delay grows linearly with the cycle duration, for all but very low values, when the average number of retransmissions is high.

Note that these values are on the low side for practical WSN duty cycle periods, as, due to the target to operate the network at low duty cycles and to ON times at least in the order of a few tens of milliseconds, the duty cycle period is usually much longer. This confirms that in practice the assumption of independent WLAN status during consecutive sensing procedures holds.

C. COG-MAC Stability

The quality of a communication protocol depends on its stability, i.e. how the selected performance metrics vary over time. A protocol with highly variable performance is not desirable. We have therefore evaluated how the number of per packet COG-MAC handshake and packet retransmission attempts vary at different WLAN observable load values. We have considered the simulation topology of Fig. 15(b) with an AP generating 50% and 5 WTs, each generating 10% of the WLAN packets. We have placed 9 RR nodes at fixed locations, such that RR sensor s_i^r observes $i \cdot 10\%$ of the WLAN active periods. For each experiment we have varied the TR location as before.

Fig. 18 depicts the coefficient of variation, $c = \sqrt{\mathrm{Var}[.]}/E[.]$, of the measured handshake and transmission attempts per packet, for different p_{CCA}^R values and under different WLAN $(p, \bar{I}^{(\mathrm{WS})})$ model parameterizations. The low coefficient of variation values – significantly below one – indicates that indeed COG-MAC does maintain a relatively stable performance with little variations across expected values. In addition, the coefficient of variation of the packet transmission attempts is lower compared with the one of the handshake attempts and almost insensitive to the p_{CCA}^R values, which confirms the efficiency COG-MAC white space discovery mechanism.

D. Multihop COG-MAC Performance Analysis

Finally, we study the impact of COG-MAC on the energy efficiency of multihop WSN communication under WLAN interference. COG-MAC with energy optimized shortest path (SP) routing is compared to a benchmark solution with CSMA/CA and the widely accepted Collection Tree Protocol (CTP) [10], that finds the shortest path with the expected number of required transmissions per packet as the link weight.

In COG-MAC the optimal packet sizes may differ for the links along a shortest path. To avoid the need for packet fragmentation, the packet size is chosen at the source node as the minimum of all optimal packet lengths along the path. Packet size is selected similarly for the benchmark system.

As shown in Fig. 19, we consider a square WSN grid with 5m inter-node distance, and a source and a destination node in the opposite corners. We place the WLAN AP in the center of the grid, and many of the WTs close to the AP, to generate a heterogeneous spectrum occupancy, with higher load around the center. We compare the performance of the two solutions for a constant $\bar{I}^{(\mathrm{WS})}$ and increasing p value, that is, increasing WLAN load. Fig. 19(a) shows the transmission paths for two case studies with $p = 0.2$ and $p = 0.8$, respectively. For

low p value, that is, low WLAN load the shortest paths are identical and traverse along the line connecting the source and destination node. For high load, however, the CSMA based solution needs to avoid the area around the AP, and redirects the transmission path to the borders, where the WLAN interference is lower. At the same time COG-MAC can safely transmit along the diagonal. Fig. 19(b) gives the normalized energy and delivery delay per transmitted bit over the source-destination transmission path. The COG-MAC based solution outperforms the benchmark system, particularly when the back-off period percentage increases but the WLAN load is still moderate. We can conclude that COG-MAC leads to significant energy savings and lower delays in multihop WSNs, and, additionally, to optimal routes that are insensitive to WLAN load changes.

X. Conclusion

In this paper we proposed COG-MAC, a cognitive MAC scheme for energy efficient WSN operation under WLAN coexistence. The proposed scheme is based on controlling the interference from the coexisting WLAN by predicting its behavior with a smart channel sensing mechanism that takes into consideration the WLAN channel usage model. Energy cost minimization is achieved by optimizing the WSN single-hop transmission distance and packet length, based on the estimated parameters of the WLAN channel usage model. To solve the optimization problem we derived an analytic model for the successful single-hop WSN packet communication. Through numerical evaluation we showed that COG-MAC significantly outperforms other MAC protocols, especially in case of severe WLAN interference. The evaluation also revealed that both COG-MAC optimization of packet size and transmission distance and smart channel sensing are key mechanisms for increasing energy efficiency. We also presented simulation results to demonstrate the accuracy of the analytic model and to show that COG-MAC achieves significant gains even in multihop environment. Consequently, COG-MAC provides a distributed solution, that exploits existing functionalities available in current commercial sensor hardware, and archives energy-efficient communications in the presence of coexisting WLAN networks.

References

[1] S. Pollin, I. Tan, B. Hodge, C. Chun, and A. Bahai, "Harmful coexistence between 802.15.4 and 802.11: A measurement-based study," in *Proceedings of the 3rd International Conference on Cognitive Radio Oriented Wireless Networks and Communications*, pp. 1–6, May 2008.

[2] S. Geirhofer, L. Tong, and B. Sadler, "Dynamic spectrum access in the time domain: Modeling and exploiting white space," *IEEE Communications Magazine*, vol. 45, pp. 66 –72, May 2007.

[3] J. Al-Karaki and A. Kamal, "Routing techniques in wireless sensor networks: a survey," *IEEE Wireless Communications*, vol. 11, pp. 6 – 28, Dec. 2004.

[4] A. Bachir, M. Dohler, T. Watteyne, and K. Leung, "MAC essentials for Wireless Sensor Networks," *IEEE Communications Surveys Tutorials*, vol. 12, no. 2, pp. 222–248, 2010.

[5] M. Buettner, G. V. Yee, E. Anderson, and R. Han, "X-MAC: a short Preamble MAC Protocol for Duty-Cycled Wireless Sensor Networks," in *Proceedings of the 4th International Conference on Embedded Networked Sensor Systems*, SenSys'06, pp. 307–320, ACM, 2006.

[6] W. Ye, F. Silva, and J. Heidemann, "Ultra-low duty cycle MAC with scheduled channel polling," in *Proceedings of the 4th international conference on Embedded networked sensor systems*, SenSys'06, pp. 321–334, ACM, 2006.

[7] F. Ashraf, R. Crepaldi, and R. Kravets, "Know your neighborhood: A strategy for energy-efficient communication," in *IEEE 7th International Conference on Mobile Adhoc and Sensor Systems (MASS'10)*, pp. 392–401, Nov. 2010.

[8] M. Di Francesco, G. Anastasi, M. Conti, S. Das, and V. Neri, "Reliability and Energy-Efficiency in IEEE 802.15.4/ZigBee Sensor Networks: An Adaptive and Cross-Layer Approach," *IEEE Journal on Selected Areas in Communications*, vol. 29, pp. 1508–1524, Sep. 2011.

[9] A. Camillò, M. Nati, C. Petrioli, M. Rossi, and M. Zorzi, "Iris: Integrated data gathering and interest dissemination system for wireless sensor networks," *Ad Hoc Networks*, vol. 11, no. 2, pp. 654–671, 2013.

[10] O. Gnawali, R. Fonseca, K. Jamieson, D. Moss, and P. Levis, "Collection tree protocol," in *Proceedings of the 7th ACM Conference on Embedded Networked Sensor Systems*, SenSys'09, pp. 1–14, ACM, 2009.

[11] L. Lo Bello and E. Toscano, "Coexistence Issues of Multiple Co-located IEEE 802.15.4/ZigBee Networks Running on Adjacent Radio Channels in Industrial Environments," *IEEE Transactions on Industrial Informatics*, vol. 5, pp. 157–167, May 2009.

[12] L. Angrisani, M. Bertocco, D. Fortin, and A. Sona, "Experimental study of coexistence issues between IEEE 802.11b and IEEE 802.15.4 Wireless Networks," *IEEE Transactions on Instrumentation and Measurement*, vol. 57, pp. 1514–1523, Aug. 2008.

[13] S. Y. Shin, H. S. Park, S. Choi, and W. H. Kwon, "Packet error rate analysis of ZigBee under WLAN and Bluetooth Interferences," *IEEE Transactions on Wireless Comm.*, vol. 6, no. 8, pp. 2825–2830, 2007.

[14] M. Hanninen, J. Suhonen, T. Hamalainen, and M. Hannikainen, "Link quality-based channel selection for resource constrained WSNs," *Springer Advances in Grid and Pervasive Computing*, vol. 6646, pp. 254–263, 2011.

[15] K. il Hwang, S.-S. Yeo, and J. H. Park, "Adaptive multi-channel utilization scheme for coexistence of IEEE 802.15.4 LR-WPAN with other interfering systems," in *Proceedings of the 11th IEEE International Conference on High Performance Computing and Communications, 2009. HPCC'09*, pp. 297–304, Jun. 2009.

[16] J. Ansari and P. Mähönen, "Channel selection in spectrum agile and cognitive mac protocols for wireless sensor networks," in *Proceedings of the 8th ACM international workshop on Mobility management and wireless access*, ACM MobiWac'10, pp. 83–90, ACM, 2010.

[17] H. Rahul, N. Kushman, D. Katabi, C. Sodini, and F. Edalat, "Learning to share: Narrowband-friendly wideband networks," *SIGCOMM Comput. Commun. Rev.*, vol. 38, pp. 147–158, Aug. 2008.

[18] K. Chowdhury and I. Akyildiz, "Interferer Classification, Channel Selection and Transmission Adaptation for Wireless Sensor Networks," in *Proceedings of IEEE International Conference on Communications*, pp. 1–5, June 2009.

[19] Y. Wu, G. Zhou, and J. Stankovic, "ACR: Active Collision Recovery in Dense Wireless Sensor Networks," in *Proceedings of IEEE International Conference on Computer Communications*, pp. 1–9, Mar. 2010.

[20] C. Liang, N. Priyantha, J. Liu, and A. Terzis, "Surviving Wi-Fi interference in low power ZigBee networks," in *Proceedings of the 8th ACM Conference on Embedded Networked Sensor Systems*, pp. 309–322, 2010.

[21] P. Rathod, O. Dabeer, A. Karandikar, and A. Sahoo, "Characterizing the exit process of a non-saturated ieee 802.11 wireless network," in *MobiHoc*, pp. 249–258, 2009.

[22] J. Misic and V. Misic, "Characterization of idle periods in IEEE 802.11e networks," in *Proceedings of IEEE Wireless Communications and Networking Conference (WCNC)*, pp. 1004–1009, Mar. 2011.

[23] S. Geirhofer, L. Tong, and B. M. Sadler, "Cognitive medium access: Constraining interference based on experimental models," *IEEE Selected Areas in Communications*, vol. 26, no. 1, 2008.

[24] L. Stabellini, "Quantifying and modeling spectrum opportunities in a real wireless environment," in *Proceedings of Wireless Communications and Networking Conference (WCNC)*, pp. 1–6, Apr. 2010.

[25] J. Huang, G. Xing, G. Zhou, and R. Zhou, "Beyond Co-existence; Exploiting WiFi White Space for ZigBee Performance Assurance," in *Proceedings of IEEE International Conference on Netw. Protocols*, 2010.

[26] S. Geirhofer, J. Z. Sun, L. Tong, and B. M. Sadler, "Cognitive frequency hopping based on interference prediction: theory and experimental results," *ACM SIGMOBILE Mob. Comput. Commun. Rev.*, vol. 13, pp. 49–61, Sep. 2009.

[27] I. Glaropoulos, V. Fodor, L. Pescosolido, and C. Petrioli, "Cognitive WSN transmission control for energy efficiency under WLAN coexistence," in *Proceedings of the 6th International Conference on Cognitive Radio Oriented Wireless Networks and Communications*, Jun. 2011.

[28] X. Liu, S. Zhang, J. Wang, J. Cao, and B. Xiao, "Anchor supervised distance estimation in anisotropic wireless sensor networks," in *Proceedings of IEEE Wireless Communications and Networking Conference (WCNC)*, pp. 938–943, Mar. 2011.
[29] C. P. from Texas Instruments, "2.4GHz IEEE 802.15.4 / ZigBee-ready RF Transceiver," tech. rep., Texas Instruments, 2008.
[30] D. Tse and P. Viswanath, *Fundamentals of Wireless Communication*. Cambridge University Press, 2005.
[31] A. Ghasemi and E. Sousa, "Collaborative spectrum sensing for opportunistic access in fading environments," in *Proceedings of the 1st IEEE International Symposium on new Frontiers in Dynamic Spectrum Access Networks (DySPAN'05)*, pp. 131–136, Nov. 2005.
[32] V. Fodor, I. Glaropoulos, and L. Pescosolido, "Detecting low-power primary signals via distributed sensing to support opportunistic spectrum access," in *IEEE International Conference on Communications*, pp. 1 –6, june 2009.
[33] I. Glaropoulos, "Energy efficient cognitive mac for sensor networks under wlan co-existence - Revised complementary technical report," tech. rep., KTH, Royal Institue of Technology, August 2013.
[34] M. Lagana, I. Glaropoulos, V. Fodor, and C. Petrioli, "Modeling and estimation of partially observed wlan activity for cognitive wsns," in *IEEE Wireless Communications and Networking Conference (WCNC)*, pp. 1526 –1531, Apr. 2012.
[35] I. Glaropoulos and V. Fodor, "Discrete stochastic optimization based parameter estimation for modeling partially observed WLAN spectrum activity," *Infocommunications Journal*, vol. 4, no. 2, pp. 11–17, 2012.
[36] P. Lin, C. Qiao, and X. Wang, "Medium access control with a dynamic duty cycle for sensor networks," in *IEEE Wireless Communications and Networking Conference (WCNC)*, vol. 3, March 2004.
[37] *NS-Miracle: Multi-InteRfAce Cross-Layer Extension library for the Network Simulator*. http://telecom.dei.unipd.it/pages/read/58/.